buildings

MDPI

Article

Mechanical Response and Deformation Evolution of Composite Linings with Prefabricated Inverts in Mining-Method Tunnels During Construction

Chengyong Chen [1], Youkai Li [2], Changjing Xu [1], Baoqun Wang [2] and Chaoqun Sun [2,*]

[1] Shandong Expressway Infrastructure Construction Co., Ltd., Jinan 250014, China; chency@163.com (C.C.); pfychenqinge@163.com (C.X.)
[2] College of Civil Engineering, Shandong Jiaotong University, Jinan 250357, China; 114008@sdjtu.edu.cn (Y.L.); 204002@sdjtu.edu.cn (B.W.)
* Correspondence: scq86320@163.com; Tel.: +86-15665869522

Abstract

To address the unclear relationship between overall deformation and local mechanical responses during the construction of composite linings consisting of precast inverts and cast-in-place arches in mining-method tunnels, this study takes Yaopocun Tunnel as the engineering case and uses field monitoring data from three typical cross-sections. Considering key construction stages, including invert segment assembly, base grouting, and casting of the secondary lining of the arch and walls, the spatiotemporal evolution of contact pressure between the invert and cushion layer, contact pressure between the secondary lining and primary support, reinforcement stress in the arch and walls, stress converted from concrete strain, and cross-sectional deformation is analyzed. The results show that variations in the contact pressure at the invert base exhibit temporal associations with construction equipment loading and subsequent secondary lining casting. The two types of interface contact pressure exhibited distinctly nonuniform distributions, with the mean monitored pressures during the later stage ranging from 30.39 to 36.47 kPa and from 52.67 to 85.16 kPa, respectively. In the later stages, the arch–wall reinforcement is predominantly under compression, with the absolute average compressive stress on the outer side being 1.32–1.99 times that on the inner side. Compressive stress is particularly pronounced at the wall feet. Although the strain-derived nominal stress responses of concrete were predominantly compressive, localized tensile responses were also identified, with a maximum calculated nominal tensile stress of approximately 2.34 MPa. The final crown settlement across the three sections ranges from 27.50 to 33.76 mm. Based on the normalized rate-of-change criterion, cross-sectional deformation entered a slowly varying stage approximately 4–5 days after invert excavation and rapid assembly, whereas interface contact pressure and lining material stress entered slowly varying stages approximately 24–40 days after subsequent secondary lining casting. These characteristic times were referenced to different construction events and do not indicate complete mechanical stabilization. These findings indicate that the overall deformation and local mechanical responses of composite linings with precast inverts exhibit distinct staged evolution patterns. A gradual stabilization of overall deformation does not necessarily indicate that subsequent adjustments in local mechanical responses have ended. During construction, attention should therefore be paid to stress variations at the wall feet and in localized tensile regions while controlling overall deformation.

Check for updates

Academic Editor: Yong Tan

Received: 14 October 2026
Revised: 27 October 2026
Accepted: 28 October 2026
Published: 29 October 2026

Copyright: © 2026 by the authors. Licensee MDPI, Basel, Switzerland. This article is an open access article distributed under the terms and conditions of the Creative Commons Attribution (CC BY) license.

Keywords: mining-method tunnels; precast inverts; field monitoring; contact pressure; construction-stage deformation

1. Introduction

The construction response of mining-method tunnels is jointly governed by surrounding rock stress release, support installation, and structural constraints. The ground pressure–convergence relationship and the convergence–confinement method link support loads to ground properties and installation stages, providing a basis for understanding load transfer during construction [1,2]. In a system consisting of primary support and secondary lining, the invert transfers loads at the tunnel bottom and contributes to circumferential closure. Consequently, its construction timing and connection method can alter subsequent loading conditions. Therefore, evaluating invert construction schemes requires simultaneous consideration of interface interactions, lining material stresses, and overall deformation, rather than relying solely on displacement at a particular construction stage to assess the structural response.

Precasting the invert and assembling it inside the tunnel may reduce the need for on-site casting and curing operations, although its relative construction efficiency depends on project-specific conditions. However, component production, lifting, joint assembly, and connection to the cast-in-place arch and wall lining introduce distinct load-transfer paths. Full-scale tests and numerical analyses by Wang revealed stress variations in precast inverts during curing and lifting, highlighting the effects of hydration heat and lifting conditions [3]. Liu Jingtang et al. evaluated the effects of segment number, thickness, and width on the deformation and damage of precast inverts for highway tunnels through comparative analysis of different design schemes [4]. Wang et al. further identified localized weak regions at joints and around the corners of central columns, as well as crack evolution, through model tests of box-shaped inverts [5]. These studies indicate that the structural configuration and construction feasibility of precast inverts should be evaluated together. Material strength or component dimensions alone are insufficient to explain the overall response of composite linings.

Connection details are critical to the collaborative behavior of precast inverts and cast-in-place arch and wall linings. Kong et al. compared internal force transfer and damage characteristics at different invert–arch–wall connections using model tests and finite element analyses that accounted for surrounding rock constraints [6]. Deng Qihua et al. investigated structural selection and circumferential connections in drill-and-blast tunnels, demonstrating that connection configurations can affect joint displacement and failure modes [7]. Regarding local shear mechanisms, Chen et al. investigated the effects of reinforcement anchorage ratio, interface dimensions, and surface treatment through direct shear tests [8], while Zhang et al. examined the effects of the pretension state of longitudinal bolted joints on slip and shear capacity [9]. These studies provide an experimental basis for connection design. However, local specimens and idealized boundary conditions cannot directly establish the pressure and stress distributions occurring during actual construction.

Related studies on segmental linings further indicate that joint rotational capacity and support from the surrounding medium jointly influence structural internal forces [10,11]. Full-scale joint tests have shown that connection details and initial contact conditions can alter nonlinear joint stiffness [12]. Analyses of contact defects have revealed links between nonuniform support, localized damage, and load-bearing behavior [13]. Full-scale tests involving multiple rings have also demonstrated the coupling between local connections, overall internal forces, and structural deformation [14]. Reinforcement stresses during con-

struction are additionally affected by load combinations and construction conditions [15], while the selection of ground–lining boundary conditions and loading models can alter calculated sectional forces [16]. These studies primarily concern circular shield-tunnel segments and provide useful mechanistic references for understanding contact and connection behavior. However, their boundary conditions, loading conditions, and quantitative parameters cannot be directly transferred to precast inverts in mining-method tunnels.

Field monitoring provides direct evidence for identifying relationships between construction events and lining responses. Zhang et al. measured the evolution of secondary lining contact pressure during the construction of a high-speed railway tunnel in loess and associated the first pressure peak with the removal of the lining formwork trolley [17]. Nine months of reinforcement strain records reported by Wu et al. revealed pronounced temporal and spatial variations in secondary lining responses [18]. Field investigations of tunnels with large spans and small clear distances further demonstrated that adjacent construction can induce internal force redistribution and spatial asymmetry in the lining [19]. Hu Xueliang et al. analyzed construction-stage pressure and internal forces in the secondary lining of a large-span tunnel, indicating that hydration effects and longitudinal construction progress both contribute to early-stage mechanical evolution [20]. These findings support the interpretation of monitoring curves with reference to specific construction events and highlight the need to evaluate average responses and local critical regions separately.

At the material scale, recent studies on self-leveling sand concrete have explored the relationships among mixture design, microstructural characteristics, mechanical performance, and durability [21,22]. The early-age behavior of concrete further complicates the interpretation of construction-stage stresses. Rankoth et al. validated a thermal stress model for secondary linings constructed using the New Austrian Tunnelling Method (NATM) by integrating field temperature, strain, and stress data. Their results indicated that the effective modulus, autogenous shrinkage, joints, and thermal boundary conditions all require consideration [23]. Nakamura et al. used field temperature measurements to identify material thermal properties and analyzed the effects of formwork removal and drying shrinkage on early cracking [24]. Numerical research by Sun et al. demonstrated that waterproofing layers and invert restraint conditions can alter the distribution of early-age thermal stresses [25]. Investigations of cracks in existing tunnels and associated model tests have also highlighted the structural significance of localized tensile stresses and the responses of arch feet and inverts [26]. Accordingly, interface pressure, reinforcement stress, concrete stress, and displacement represent different aspects of structural behavior. A leveling-off of the deformation curve alone cannot establish that stresses in all regions have stabilized or that the concrete has remained free from cracking throughout the construction process.

In addition to conventional field monitoring, data-driven approaches have been increasingly applied to structural health monitoring and damage assessment. Khatir et al. [27] integrated experimental modal analysis, numerical simulation, and a hybrid SSA-SCA-XGBoost model to evaluate structural damage and stiffness recovery in composite-patched plates. Khatir and Capozucca [28] systematically reviewed the applications of artificial, convolutional, and deep neural networks in structural health monitoring, highlighting the potential of intelligent methods for damage identification and assessment. These developments provide complementary approaches for interpreting structural response data, alongside conventional monitoring of contact pressure, material stresses, and deformation in civil engineering structures.

More recently, Wang et al. and Hu et al. combined numerical analysis with in situ testing to investigate a novel precast invert for a NATM tunnel, monitoring settlement, convergence, interface pressure, and material responses [29,30]. Existing field evidence indicates that precast inverts should be evaluated as part of a composite system interacting

with the cast-in-place arch and wall lining and the underlying support. Nevertheless, several questions remain under different structural configurations and construction conditions: How do construction events correspond temporally to changes in the two types of interface pressure? Do the spatial distributions of interface pressure correspond to those of material stresses on the inner and outer sides of the arch and walls? Can the gradual stabilization of overall deformation after invert construction be taken to indicate that the forces in the subsequently cast secondary lining have also stabilized? Addressing these questions requires cross-checking multiple monitoring indicators against construction timelines and cross-sectional locations, rather than drawing conclusions solely from joint load-bearing tests or final displacement measurements.

Previous studies have made substantial progress in the structural design of precast inverts, joint connection performance, construction-stage mechanical responses, and early-age lining behavior [3–27]. In particular, previous investigations have examined the mechanical performance of precast invert systems using numerical analyses, experimental tests, and field monitoring. However, for composite lining systems consisting of precast inverts and cast-in-place arch and wall linings, the relationships among different mechanical response indicators during successive construction stages remain insufficiently characterized. Specifically, the spatial correspondence between interface contact pressure and internal reinforcement and concrete stresses, as well as the temporal relationship between overall deformation and subsequent local stress adjustments, requires further investigation. These issues are important because different monitoring indicators represent distinct aspects of structural behavior and may not exhibit consistent spatial distributions or temporal evolution. Therefore, a construction-stage assessment integrating multiple field monitoring indicators is needed to clarify their complementary roles and improve the interpretation of composite lining responses.

Accordingly, this study investigates the construction-stage mechanical behavior of a composite lining incorporating a precast invert in Yaopocun Tunnel, based on archived field monitoring data and construction records from three representative cross-sections. The specific contribution of this study lies in the integrated interpretation of multiple mechanical response indicators with respect to their spatial locations and corresponding construction events. First, the stage-dependent evolution and transverse distributions of two types of interface contact pressure, namely the invert–cushion and secondary lining–primary support pressures, are examined to characterize their spatial nonuniformity. Second, interface contact pressure is compared with reinforcement and concrete stresses on the inner and outer sides of the arch and walls to investigate whether local interface pressure can adequately reflect the internal mechanical state of the lining. Third, crown settlement and horizontal convergence are examined in relation to the subsequent evolution of interface pressure and material stress to identify differences in their characteristic response stages. Through these analyses, this study provides project-specific evidence of the spatial and temporal differences among multiple monitoring indicators and offers a basis for developing more comprehensive construction-stage monitoring strategies for composite linings with precast inverts.

2. Engineering Project and Archived Data Analysis Methods

2.1. Data Sources and Engineering Conditions

Yaopocun Tunnel has a total length of 154 m. The ground surface elevation in the tunnel area ranges from 1380 to 1417 m, with a relative elevation difference of approximately 37 m. The entrance and exit are located on sloping terrain with gradients of approximately 20° and 30°, respectively. The tunnel mainly passes through mudstone interbedded with sandstone, while the entrance and exit sections consist of loess and colluvial soil. Groundwater conditions generally range from water-poor to weakly water-rich. Within the tunnel, the 55 m

section from ZK20 + 732 to ZK20 + 787 adopts a composite lining system consisting of an integral precast invert and a cast-in-place secondary lining for the arch and walls. Three representative monitoring cross-sections, located at ZK20 + 732, ZK20 + 772, and ZK20 + 783, were selected within this section and designated S1, S2, and S3, respectively. The distance between the first and last monitoring cross-sections is 51 m, which should be distinguished from the total tunnel length and the length of the precast invert construction section.

The cross-sectional structure of the composite lining incorporating the precast invert is shown in Figure 1. The secondary lining of the arch and walls is made of C40 concrete, with HRB400 reinforcing bars of 20 mm diameter used for both the inner and outer main reinforcement. The composite lining consists of an integral precast invert and the upper cast-in-place arch and wall lining, which are integrated into a single structural system through reserved connection details and cast-in-place concrete.

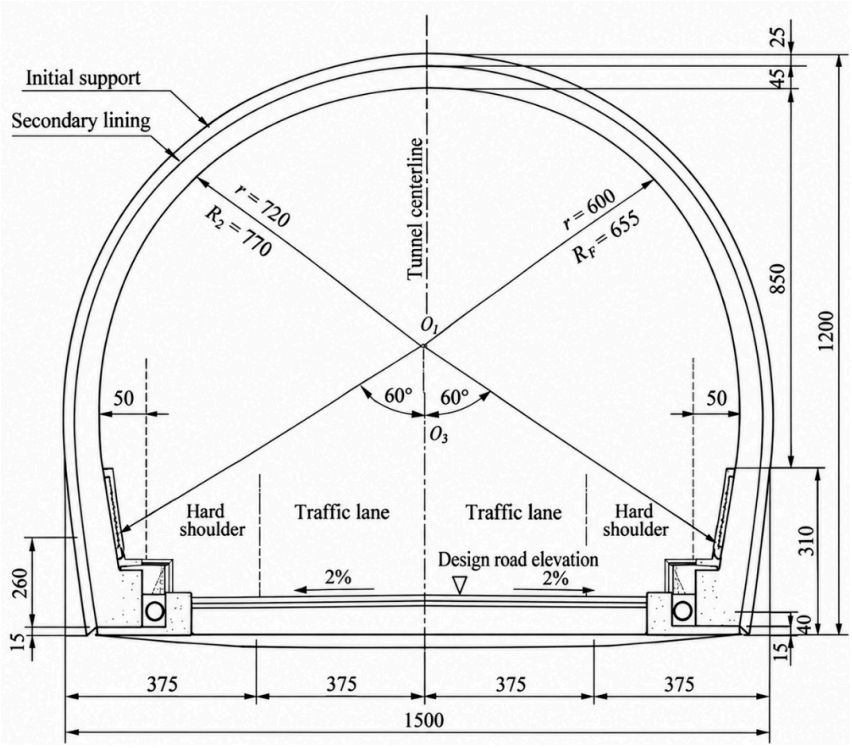


Figure 1. Cross-sectional view of the segmental precast invert (dimensions in cm).

The integral precast invert adopts a three-dimensional box-shaped structure, as shown in Figure 2. The bottom of each precast segment has a ring-shaped configuration, with dimensions of 5.744 m × 1.500 m × 1.334 m and a mass of 16.12 t. Two segments are installed during each assembly cycle. Four embedded lifting inserts, which also serve as grouting holes, are provided at the top of each segment, while three additional embedded bolt inserts are arranged at the bottom to meet the requirements for component production, lifting, and subsequent grouting operations.

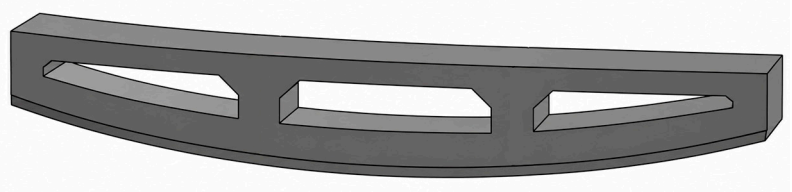


Figure 2. Three-dimensional model of the integral precast invert component.

A 150 mm thick crushed stone cushion layer is installed beneath the precast invert. Graded crushed stone or pea gravel with a particle size of 3–5 cm is used to provide a supporting interface for the bottom of the precast components. Adjacent precast segments are connected and secured using longitudinal fastening devices. The prestressing bars are 25 mm diameter threaded steel bars with a tensile strength of 785 MPa, which are tightened according to the specified thread design, with the tightening force controlled at 350 kN. During assembly, the gaps between adjacent components are maintained at 2.0–3.0 mm, while both vertical elevation differences and horizontal deviations are controlled within ± 2.0 mm to satisfy the required assembly tolerances. After installation, grouting is performed beneath the invert, with a specified terminal grouting pressure of 0.2 MPa. The secondary lining of the arch and walls is constructed only after the concrete has reached an age of at least 14 days.

The precast invert and the cast-in-place arch and wall lining are integrated into a composite lining system through dowel anchorage, reinforcement connections, and cast-in-place concrete. Dowel anchors are installed at the connections between the precast invert and the walls to ensure continuity between structural components. The primary support mainly consists of C25 shotcrete, an 8 mm diameter HPB300 reinforcing mesh, 22 mm diameter HRB400 mortar anchors or 25 mm diameter hollow anchors, and I18 steel arches. The tunnel is excavated using the upper, middle, and lower bench methods. After invert excavation, the precast components are assembled, followed by construction of the secondary lining of the arch and walls. As invert assembly, base grouting, and secondary lining casting proceed sequentially, the structural constraints and load-transfer paths of the composite lining change with each construction stage. This provides the engineering basis for subsequent analysis of the staged evolution of interface contact pressure, lining material stresses, and cross-sectional deformation.

2.2. Measurement Points and Monitoring Indicators

To investigate the mechanical behavior and deformation characteristics of the composite lining comprising the precast invert and cast-in-place arch and wall lining during construction, field monitoring systems were installed at three representative cross-sections, designated S1, S2, and S3. The monitoring parameters mainly included contact pressure between the invert and cushion layer, contact pressure between the secondary lining of the arch and walls and the primary support, reinforcement stress in the secondary lining, concrete strain, and cross-sectional deformation. By comparing monitoring results from different construction stages and structural locations, the staged variations in interfacial load transfer, internal material stresses, and overall deformation of the composite lining were analyzed.

The measurement-point arrangements at each cross-section are shown in Figure 3. Five contact pressure measurement points were installed between the precast invert and the underlying cushion layer, located sequentially at the left outer, left inner, central, right inner, and right outer positions along the cross-section. These points were used to monitor the contact pressure beneath the precast invert and its transverse distribution.

Seven monitoring locations were established in the secondary lining of the arch and walls: the left wall foot, left sidewall, left haunch, crown, right haunch, right sidewall, and right wall foot. One contact pressure cell was installed at each location. Reinforcement stress gauges and embedded concrete strain gauges were also installed on the inner and outer sides of the lining to measure interface contact pressure, reinforcement stress, and concrete strain at different locations. The inner side refers to the side facing the tunnel interior, while the outer side refers to the side adjacent to the primary support. This paired monitoring

arrangement enables comparison of material stress differences across the thickness of the secondary lining.

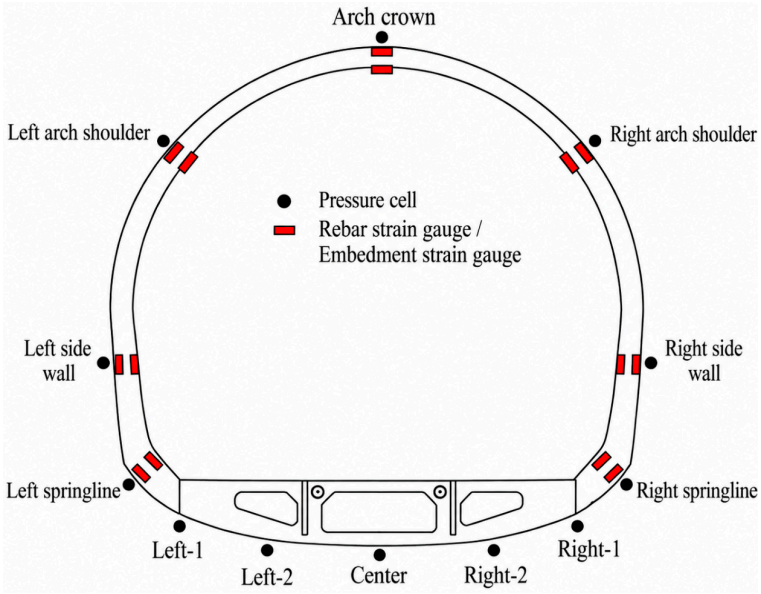


Figure 3. Layout of monitoring points for the composite lining with precast invert.

Cross-sectional deformation monitoring mainly includes crown settlement and horizontal convergence, with the measurement point arrangement shown in Figure 4. A crown settlement measurement point (GD) was installed at the tunnel crown to record changes in its vertical displacement. Horizontal convergence measurement lines SL01–SL02, SL03–SL04, and SL05–SL06 were arranged at the upper, middle, and lower benches, respectively, to monitor horizontal deformation at different excavation heights. Deformation measurements were conducted progressively during bench excavation, invert construction, and secondary lining installation to characterize the cumulative and stage-dependent changes in cross-sectional deformation caused by construction disturbances and the formation of the support structure.

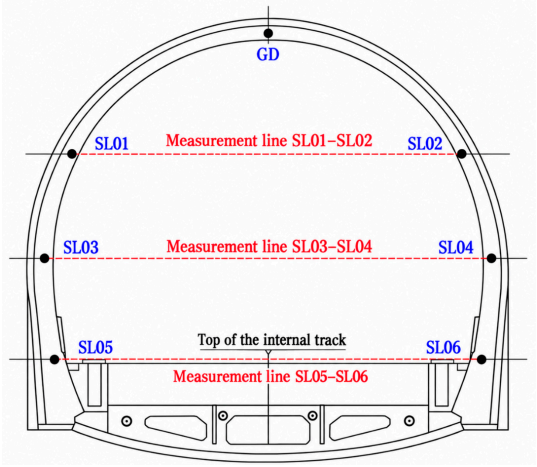


Figure 4. Layout of monitoring points for crown settlement and horizontal convergence at different benches.

The field monitoring program employed pressure cells, reinforcement stress gauges, and embedded concrete strain gauges. The main instrument models and technical specifications are listed in Table 1. The contact pressure cells were used to monitor normal contact

pressure at different structural interfaces, while the reinforcement stress gauges measured the stress responses of the inner and outer reinforcement in the secondary lining of the arch and walls. The embedded strain gauges were used to measure changes in concrete strain. Concrete stress was calculated from the measured strain and the corresponding material parameters. The data processing and analysis methods are described in Section 3.2.

Table 1. Main specifications of the monitoring instruments.

Monitoring Parameter	Instrument Model	Measurement Range	Sensitivity	Operating Temperature Range
Interface contact pressure	SZZX-EA05 pressure cell	0.5 MPa	0.001 MPa	−20 to 80 °C
Reinforcement stress	SZZX-C20B reinforcement stress gauge	±260 MPa	0.001 MPa	−20 to 80 °C
Concrete strain	SZZX-A150D embedded strain gauge	±1500 με	1 με	−20 to 80 °C

Note: Sensitivity is an instrument specification and should not be interpreted as the measurement uncertainty of the entire field monitoring system.

To ensure effective contact between the monitoring instruments and the structure, the gravel cushion layer was locally leveled before installing the pressure cells beneath the invert. Installation grooves matching the dimensions of the pressure cells were prepared at the corresponding measurement locations, and the sensor cables were routed through reserved cable channels to a collection point near the drainage ditch. The contact pressure cells for the arch and walls were installed after completion of the waterproofing layer and placed in close contact with it to monitor the interface pressure between the secondary lining and the primary support. The reinforcement stress gauges were installed on the inner and outer main reinforcement of the secondary lining of the arch and walls. They were fixed by intermittent welding and supplementary fastening measures to minimize the effects of welding heat on the instruments. The embedded concrete strain gauges were secured at the corresponding locations within the reinforcement cages and positioned at a certain distance from the reinforcement stress gauges to measure the concrete strain response at the corresponding locations.

Field monitoring data were collected using an SZDQ-ZH integrated readout unit. According to the construction event annotations in the archived monitoring plots, the precast invert assembly dates for sections S1, S2, and S3 were 16 January, 17 January, and 18 January, respectively. The corresponding base grouting dates were 16 March, 17 March, and 17 March, while the casting dates of the secondary lining of the arch and walls were 4 May, 4 May, and 8 May, respectively. These construction events provide temporal references for analyzing stage-dependent variations in interface pressure and material stress. Because the precast invert components had already been manufactured when the field monitoring scheme was established, reinforcement stress gauges and concrete strain gauges were not embedded in the components during production. Therefore, the material stress analysis in this study focuses primarily on the cast-in-place secondary lining of the arch and walls, while the precast invert is evaluated mainly based on the monitored base contact pressure.

2.3. Monitoring Data Processing and Analysis Methods

To systematically investigate the mechanical response of the composite lining incorporating a precast invert during construction, field construction records and monitoring results were combined to classify and organize interface contact pressure, reinforcement stress, concrete stress, and cross-sectional deformation at three representative cross-sections. The

analysis focused on three aspects: evolution across construction stages, spatial distribution across the cross-section, and differences in responses among monitoring indicators.

According to the field construction sequence, the monitoring process was divided into the main stages of bench excavation, invert assembly and precast component installation, base grouting, and secondary lining construction of the arch and walls. Key construction events at each stage were used as temporal references to analyze changes in contact pressure, material stress, and cross-sectional deformation. Interface contact pressure and material stress were primarily analyzed in relation to key events, including invert assembly, construction equipment loading, and secondary lining casting. Crown settlement and horizontal convergence were evaluated in relation to bench excavation and invert construction. Because the monitoring indicators correspond to different construction starting points, their stage-dependent variations were analyzed separately, without directly comparing response durations quantitatively across different starting times.

To characterize the monitored contact pressure levels at different interfaces, the arithmetic mean of the pressure measurements was calculated for each cross-section. Five monitoring points were arranged at the invert–cushion interface, while seven monitoring points were arranged at the secondary lining–primary support interface. The mean monitored pressure was calculated as follows:

$$\overline{P} = \frac{1}{n}\sum_{i=1}^{n} P_i \tag{1}$$

where the mean monitored pressure is expressed in kPa, the individual pressure measurement represents the value recorded at the corresponding monitoring point, and the number of monitoring points is denoted by n. As the monitoring points represent discrete locations along the interfaces, the arithmetic mean characterizes the average pressure level of the sampled points rather than the area-weighted mean pressure over the entire contact surface. The spatial distributions and local extreme values were therefore examined together with the mean monitored pressures to characterize interfacial contact conditions.

For the material stresses in the secondary lining of the arch and walls, tensile stress was defined as positive and compressive stress as negative. The stress distributions of the reinforcement and concrete at different monitoring locations were analyzed separately. Reinforcement stress was evaluated primarily using the average values on the inner and outer sides, local extreme values, and their locations. The ratio of the absolute average stress on the outer side to that on the inner side was used to characterize differences in reinforcement stress across the lining thickness. Concrete stress was calculated from the relationship between strain and elastic modulus, as expressed by

$$\sigma_c = E_c \varepsilon_c \tag{2}$$

where σ_c is the nominal concrete stress calculated from the measured strain (MPa); E_c is the reference elastic modulus of concrete (MPa); and ε_c is the measured concrete strain used for stress conversion. The secondary lining of the arch and walls was constructed using C40 concrete. According to the Chinese concrete design standard [31], a reference elastic modulus of 32.5 GPa was adopted for the strain-to-stress conversion. Because the age-dependent evolution of the concrete elastic modulus was not independently measured, this reference value was treated as constant throughout the analysis.

This linear–elastic relationship was adopted to characterize the apparent stress responses at different monitoring locations. It should be noted that, during the early-age period, the measured concrete strain may be influenced not only by mechanical loading but also by temperature variations, autogenous and drying shrinkage, creep, and evolving structural restraint conditions. Furthermore, the elastic modulus of concrete changes with

age. As these time-dependent effects could not be independently quantified using the available monitoring data, the calculated stresses should be interpreted as approximate strain-derived indicators rather than direct measurements of the actual mechanical stresses. Accordingly, the analysis focuses primarily on the temporal evolution, spatial differences, and potentially critical regions of the concrete response.

For cross-sectional deformation, cumulative deformation, maximum deformation rate, and stage-dependent variations in crown settlement and horizontal convergence at the upper, middle, and lower benches were extracted and analyzed in conjunction with construction events. The final deformation and stage-dependent responses of different cross-sections were compared to evaluate the overall deformation evolution during construction. Cross-sectional deformation was also compared with changes in interface contact pressure and material stress, with particular attention to the relationship between the gradual stabilization of overall deformation and the continued adjustment of local mechanical responses.

To quantitatively identify the onset of stage-wise stabilization, a normalized rate-of-change criterion was adopted for the monitoring data. For each monitoring point, the absolute rate of change and its normalized value were calculated using Equations (3) and (4), respectively.

$$v_{j,i} = \frac{\left|X_j(t_i) - X_j(t_{i-1})\right|}{t_i - t_{i-1}} \tag{3}$$

$$R_{j,i} = \frac{v_{j,i}}{v_{j,max}} \tag{4}$$

where $X_j(t_i)$ is the measured value at monitoring point j and time t_i; $v_{j,i}$ is the absolute rate of change between consecutive valid measurements; $v_{j,max}$ is the maximum absolute rate recorded at the same monitoring point during the corresponding continuous construction stage; and $R_{j,i}$ is the normalized rate of change. A monitoring point was considered to have entered a slowly varying stage when $R_{j,i}$ remained at or below 0.10 for three consecutive valid monitoring intervals spanning at least seven days. At the cross-sectional level, at least 80% of the available monitoring points for the corresponding indicator were required to satisfy this criterion. The onset time was identified retrospectively from the beginning of the first qualifying low-rate period after its persistence had been confirmed. Monitoring interruptions were excluded without interpolation. The identified time therefore represents the onset of a slowly varying response stage rather than complete mechanical stabilization, as subsequent local adjustments may still occur.

In the analysis of the monitoring results, the recorded extreme values during the monitoring period and the measurement values at cross-sectional monitoring points in the later stages were used to characterize the mechanical responses at different stages. For periods with monitoring interruptions, no data interpolation or inference of continuous responses was performed. In particular, changes in invert contact pressure during base grouting were analyzed using the available monitoring results before and after grouting. The pressure difference between different observation times was not directly interpreted as the instantaneous pressure increment caused by grouting. Based on these methods, the interfacial load transfer, material stress distribution, and cross-sectional deformation characteristics of the composite lining incorporating a precast invert during construction were comprehensively evaluated.

3. Analysis of Monitoring Results

3.1. Contact Response Between the Invert and Cushion Layer

The contact pressure between the precast invert and the underlying cushion layer exhibited pronounced stage-dependent variations during construction, with distinct responses at different monitoring locations. Figure 5 presents the contact pressure histories at the

three representative cross-sections. Following the completion of precast segment assembly, the contact pressure remained relatively low before undergoing several subsequent adjustments. In particular, increases in contact pressure were recorded at some monitoring points following the entry of a 23 t excavator into the invert construction area, while decreases were observed after the equipment left. Further increases at certain monitoring points coincided with the arrival of the secondary lining formwork trolley. Compared with section S1, sections S2 and S3 exhibited more pronounced pressure variations during this period. These observations reveal temporal associations between construction activities and changes in invert contact pressure. Although temporary construction loads may contribute to the observed variations, their individual effects cannot be independently quantified from the available monitoring data. Therefore, the pressure changes are interpreted as stage-dependent monitoring responses rather than direct evidence of specific equipment-induced load increments.

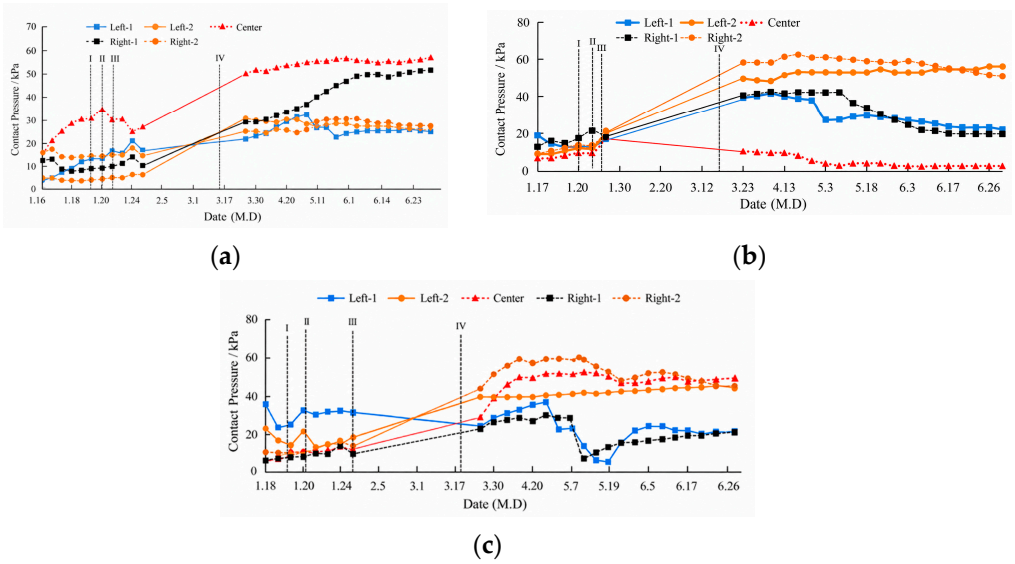


Figure 5. Contact pressure between the invert and cushion layer: (**a**) ZK20 + 732; (**b**) ZK20 + 772; (**c**) ZK20 + 783.

As construction progressed, the contact pressure at the base of the invert exhibited further variations. As shown in Figure 5, contact pressure monitoring was interrupted between January 26 and March 22, during which base grouting was performed. Consequently, the immediate pressure response associated with grouting could not be captured. Comparison of the available measurements before the interruption and after monitoring resumed revealed differences in contact pressure levels and spatial distributions at several monitoring points. However, these differences represent the overall changes occurring during the unmonitored period and cannot be attributed exclusively to the grouting operation, as other construction activities and changes in interface support conditions may also have contributed. Therefore, the available data are used only to characterize the differences in contact conditions between the two observation periods, rather than to quantify the pressure increment induced by grouting. The peak contact pressures recorded during the monitoring period at sections S1, S2, and S3 were 58.11, 66.01, and 59.09 kPa, respectively. The maximum value at section S1 occurred at the center of the invert, whereas those at sections S2 and S3 occurred at the Right-2 measurement point. The corresponding results are presented in Table 2.

Table 2. Recorded peak contact pressures at the two interfaces and time to stage-wise stabilization.

Section	Interface	Peak Pressure (kPa)	Peak Location	Onset of Slowly Varying Stage After Secondary Lining Casting (d)
S1	Invert–cushion layer	58.11	Invert center	24
S2	Invert–cushion layer	66.01	Right-2	29
S3	Invert–cushion layer	59.09	Right-2	25
S1	Secondary lining–primary support	171.22	Left haunch	40
S2	Secondary lining–primary support	83.87	Crown	30
S3	Secondary lining–primary support	104.25	Right sidewall	40

After casting the secondary lining of the arch and walls, the contact pressure at the invert base continued to vary. Pressure reductions occurred at some measurement points on both sides, particularly near the arch–wall connection regions, indicating a further adjustment in the base contact pressure during subsequent lining construction. As construction progressed, the magnitude of pressure variations at each monitoring point gradually decreased. Based on the normalized rate-of-change criterion described in Section 2.3, the contact pressure responses at sections S1, S2, and S3 entered a slowly varying stage approximately 24, 29, and 25 days, respectively, after casting of the secondary lining of the arch and walls. These characteristic times represent the onset of reduced pressure variation rather than the complete cessation of subsequent adjustments. These results indicate that the contact response at the invert base is associated not only with precast component assembly but also with construction equipment loading and the subsequent construction of the arch and wall lining.

To further investigate the transverse distribution of contact pressure at the invert–cushion interface, the measurements obtained during the later monitoring stage were compared among the three cross-sections, as shown in Figure 6 and Table 3. The arithmetic mean pressures at the monitored locations of sections S1, S2, and S3 were 36.47, 30.39, and 35.27 kPa, respectively. Although the mean values were relatively close, considerable differences were observed among individual monitoring points. At section S1, the maximum pressure was 57.28 kPa at the Right-2 position, while the minimum was 23.63 kPa at the center. At section S2, the maximum pressure was 56.06 kPa at the Left-2 position, while the minimum was 2.76 kPa at the center, indicating a pronounced transverse variation. At section S3, the maximum pressure was 48.36 kPa at the center of the invert, while the minimum was 19.14 kPa at the Left-1 position. These results indicate that the principal load-bearing locations differ among the cross-sections. The higher pressures at sections S1 and S2 were mainly distributed at the intermediate measurement points on both sides, whereas the higher pressure at section S3 occurred in the central region.

Table 3. Cross-sectional characteristics of contact pressure at the two interfaces during the later stage.

Section	Interface	Mean Monitored Pressure (kPa)	Maximum Pressure and Location (kPa)	Minimum Pressure and Location (kPa)
S1	Invert–cushion layer	36.47	57.28, Right-2	23.63, Center
S2	Invert–cushion layer	30.39	56.06, Left-2	2.76, Center
S3	Invert–cushion layer	35.27	48.36, Center	19.14, Left-1
S1	Secondary lining–primary support	85.16	112.12, Left haunch	42.35, Right wall foot
S2	Secondary lining–primary support	52.67	77.63, Crown	21.32, Right wall foot
S3	Secondary lining–primary support	62.05	88.68, Crown	25.26, Right wall foot

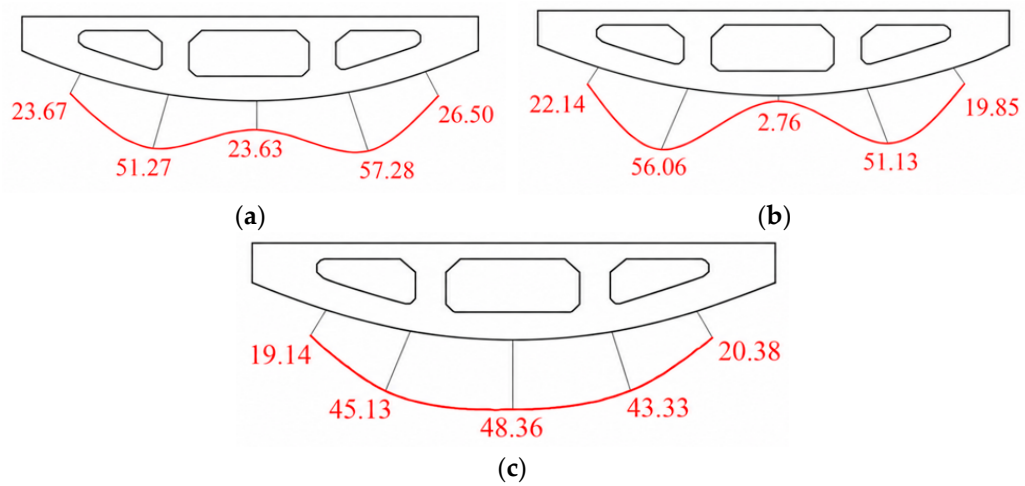


Figure 6. Transverse distribution of contact pressure at the invert–cushion interface during the later monitoring stage (kPa): (**a**) ZK20 + 732; (**b**) ZK20 + 772; (**c**) ZK20 + 783.

Overall, the contact pressure between the precast invert and the underlying cushion layer exhibits pronounced dependence on construction stages and spatial nonuniformity. On the one hand, construction equipment loading and subsequent casting of the secondary lining of the arch and walls are both accompanied by local adjustments in contact pressure. On the other hand, although the average pressures differ relatively little among the cross-sections, the local extreme values and their locations vary considerably. These findings indicate that a uniform pressure assumption cannot adequately characterize the actual contact conditions beneath the invert. Therefore, the mechanical behavior of the precast invert during construction should be evaluated by considering pressure variations at different transverse locations.

3.2. Contact Pressure Between the Secondary Lining and Primary Support

The contact pressure between the secondary lining of the arch and walls and the primary support is an important indicator of the mechanical state at the lining interface. The contact pressure histories for the three representative cross-sections are shown in Figure 7. Following casting of the secondary lining, the contact pressure at most monitoring locations exhibited staged variations characterized by rapid increases, local decreases, and gradual subsequent adjustments. However, the pressure increases and local responses differed among the cross-sections. During the initial stage after casting, the contact pressure increased rapidly at some monitoring points, reaching peak values during the monitoring period approximately 5–8 days after casting. Subsequently, the pressure gradually decreased at some locations, while it continued to increase slowly or remained relatively stable at others. These variations indicate that the interfacial mechanical state between the secondary lining and primary support continued to adjust during construction.

Among the three cross-sections, the maximum contact pressures recorded during the monitoring period were 171.22 kPa at the left haunch of S1, 83.87 kPa at the crown of S2, and 104.25 kPa at the right sidewall of S3. The differences in both magnitude and location indicate pronounced spatial heterogeneity in the contact response between the secondary lining and primary support. At S1, the pressure evolution at the left wall foot also differed from that at other monitoring locations, further reflecting the localized nature of interfacial contact conditions. As the interface conditions continued to evolve after secondary lining casting, the pressure variation rates gradually decreased. According to the normalized rate-of-change criterion, the contact pressure responses at sections S1, S2, and S3 entered slowly varying stages approximately 40, 30, and 40 days after casting, respectively. These

times characterize the transition to a slower response stage, during which further local pressure adjustments may still occur. The corresponding peak pressures and characteristic times are presented in Table 2.

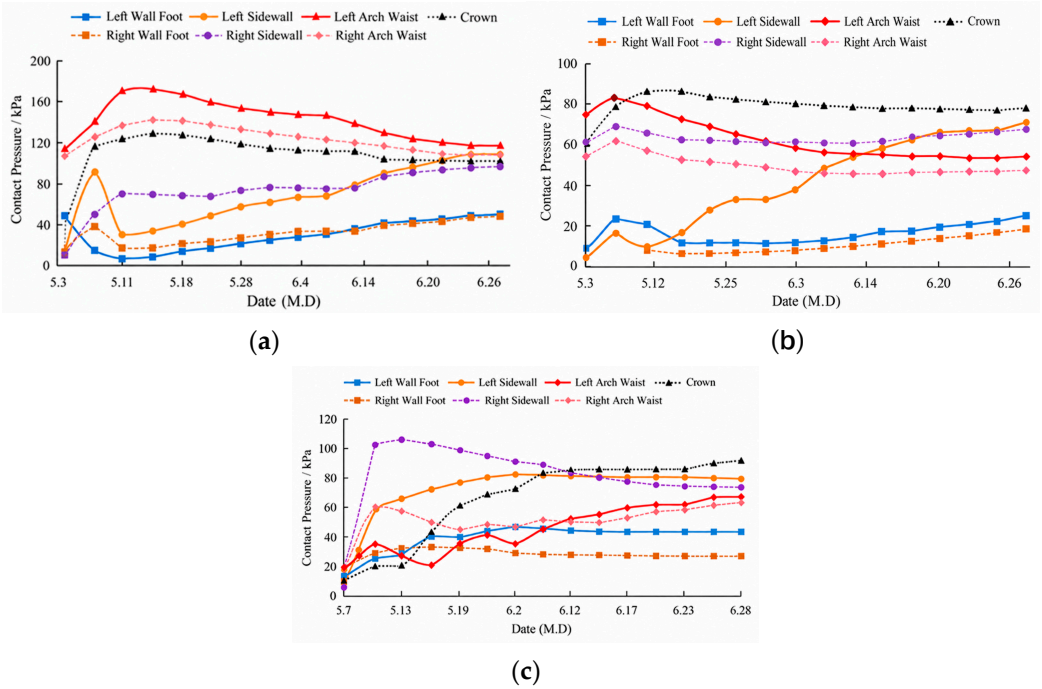


Figure 7. Time histories of contact pressure between the secondary lining of the arch and walls and the primary support: (**a**) ZK20 + 732; (**b**) ZK20 + 772; (**c**) ZK20 + 783.

To further investigate the contact pressure distribution between the secondary lining and primary support, the measurements obtained during the later monitoring stage were compared among the three cross-sections, as shown in Figure 8 and Table 3. The arithmetic mean pressures at the monitored locations of sections S1, S2, and S3 were 85.16, 52.67, and 62.05 kPa, respectively. Section S1 exhibited the highest mean monitored pressure, whereas S2 exhibited the lowest, indicating differences in the contact pressure levels recorded at the selected monitoring locations. The arithmetic means at the secondary lining–primary support interface were also higher than those at the invert–cushion interface. However, because the two interfaces differ in geometry, contact area, pressure direction, and monitoring-point arrangement, these mean values should be interpreted as statistical characteristics of the measured pressures rather than direct indicators of the total contact forces or load-sharing proportions of the structural components.

In terms of the spatial distribution across the cross-section, the contact pressure between the secondary lining of the arch and walls and the primary support was markedly nonuniform. Higher pressures were mainly distributed at the haunches, crown, and sidewalls, whereas relatively lower contact pressures occurred at the wall feet. At section S1, the maximum contact pressure during the later stage was 112.12 kPa at the left haunch, while the minimum was 42.35 kPa at the right wall foot. At section S2, the maximum was 77.63 kPa at the crown, and the minimum was 21.32 kPa at the right wall foot. At section S3, the maximum was 88.68 kPa, also at the crown, while the minimum was 25.26 kPa at the right wall foot. Although the locations of maximum pressure differed among the three sections, the minimum pressure occurred at the right wall foot in all three, indicating a common spatial characteristic.

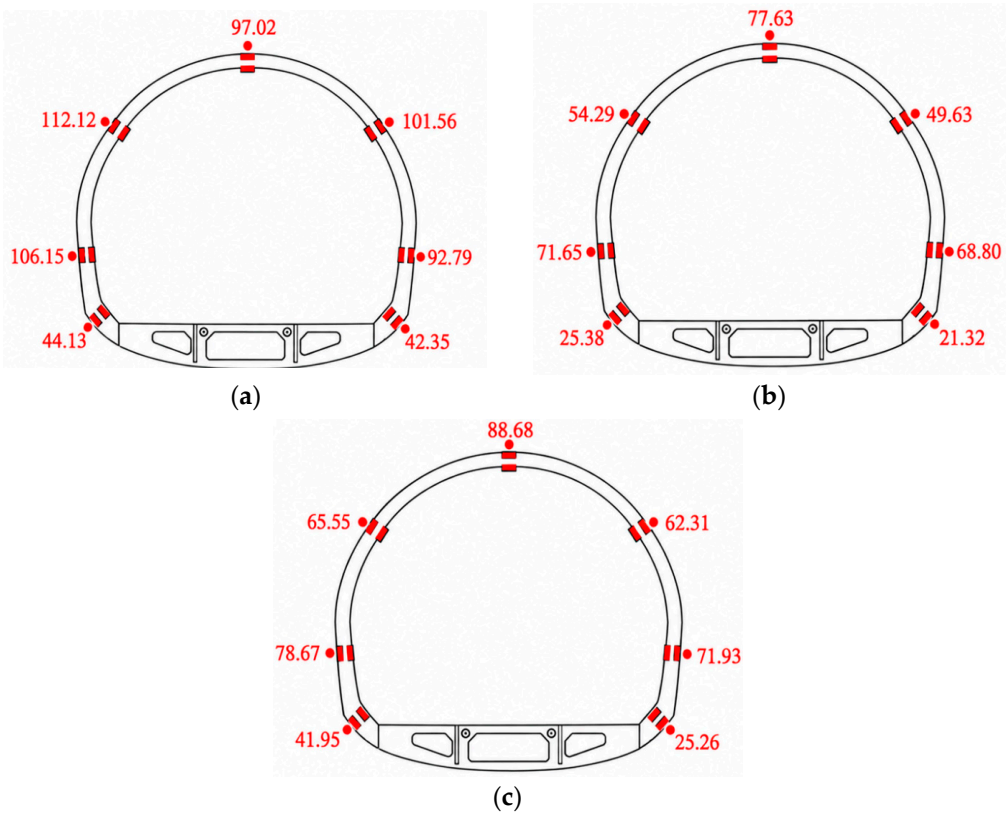


Figure 8. Cross-sectional distribution of contact pressure between the secondary lining of the arch and walls and the primary support during the later stage (kPa): (**a**) ZK20 + 732; (**b**) ZK20 + 772; (**c**) ZK20 + 783.

Further comparison of contact pressures at different structural locations shows that the average pressure at the wall feet ranged from 23.35 to 43.24 kPa across the three sections, substantially lower than the average pressure of 70.23–99.47 kPa at the sidewalls. Compared with the sidewalls and some arch regions, the wall feet were subjected to relatively lower local normal contact pressure. This indicates significant variation in interfacial interaction along the lining perimeter, with lower contact pressures at the wall feet coexisting with higher pressures at adjacent sidewall locations. In addition, pressure differences between corresponding locations on the left and right sides were observed, indicating that the interface pressure distribution was not strictly symmetrical.

Overall, the contact pressure between the secondary lining of the arch and walls and the primary support exhibits pronounced variations across construction stages and a nonuniform spatial distribution along the cross-section. Following secondary lining casting, the interface contact pressure initially increases rapidly and then gradually enters a stage of slower adjustment. The magnitude of the changes and the locations of local extreme values vary among the monitoring cross-sections. Relatively low contact pressures at the wall feet, together with higher pressures at the haunches, crown, and sidewalls, form a nonuniform interfacial stress state. Since interface contact pressure reflects only local normal contact forces and cannot directly characterize the internal stress state of the reinforcement and concrete, subsequent material stress monitoring results are required to further investigate the relationship between the internal forces in the secondary lining and the interface contact pressure.

3.3. Reinforcement Stress in the Secondary Lining of the Arch and Walls

The reinforcement stress in the secondary lining of the arch and walls exhibits pronounced stage-dependent variations during construction, with differences in stress responses among monitoring locations and between the inner and outer sides of the lining. The reinforcement stress histories for the three representative cross-sections are shown in Figure 9. Overall, the reinforcement in the secondary lining was predominantly under compression during the monitoring period. Following secondary lining casting, the compressive stress in the reinforcement generally increased and subsequently underwent varying degrees of adjustment as construction progressed. Short-term tensile stresses occurred at some monitoring points during the initial casting stage. The maximum tensile stresses in the inner and outer reinforcement at the crown of section S1 were 0.28 and 1.09 MPa, respectively, while the maximum tensile stress in the outer reinforcement at the left haunch of section S3 was 0.15 MPa. These stresses subsequently transitioned to compression. Compared with the inner reinforcement, the outer reinforcement generally exhibited greater stress variations, indicating differences in the stress state across the lining thickness.

In terms of the stress variations at different monitoring locations, the absolute values of compressive stress in the reinforcement at the wall feet and sidewalls were generally higher than those at the haunches and crown. Following secondary lining casting, the compressive stress in the reinforcement at some wall-foot locations increased rapidly and subsequently entered a stage of relatively gradual adjustment. The three cross-sections exhibited broadly similar stress variation trends, although the local peak compressive stresses and their locations differed. The maximum absolute compressive stress in the outer reinforcement at section S1 was 23.26 MPa. At section S2, it was 27.81 MPa at the outer reinforcement of the left wall foot. At section S3, it reached 31.51 MPa at the outer reinforcement of the right wall foot, the highest recorded value among the three cross-sections. These results indicate that the wall feet are regions of pronounced reinforcement compression, while the local stress levels and distribution patterns vary among the cross-sections.

To further investigate the spatial distribution of reinforcement stress in the secondary lining of the arch and walls, the inner and outer reinforcement stresses during the later monitoring stage were compared for the three cross-sections, as shown in Figure 10. The reinforcement at all monitoring points was under compression during the later stage. However, the stress distribution was not completely symmetrical, and pronounced differences existed between the inner and outer reinforcement. The maximum absolute compressive stresses in the inner and outer reinforcement at section S1 were 16.50 and 23.26 MPa, respectively. At section S2, the corresponding values were 25.81 and 27.81 MPa, while at section S3, they were 12.34 and 31.51 MPa. The difference between the maximum absolute compressive stresses in the inner and outer reinforcement was particularly pronounced at section S3, indicating substantial local variations in reinforcement stress among different cross-sections and structural locations.

Further statistical analysis of the average reinforcement stresses and local extreme values at the three cross-sections is presented in Table 4. The average compressive stresses in the inner-side reinforcement at sections S1, S2, and S3 were −9.65, −11.50, and −7.93 MPa, respectively, while those in the outer-side reinforcement were −12.76, −16.65, and −15.76 MPa, respectively. At all three cross-sections, the absolute average compressive stress in the outer-side reinforcement exceeded that in the inner-side reinforcement. The ratios of the absolute average compressive stress on the outer side to that on the inner side were 1.32, 1.45, and 1.99, respectively. These results indicate pronounced stress differences across the lining thickness, with the outer-side reinforcement generally experiencing greater compression. However, the magnitude of this difference varied among the cross-sections. The difference between the average compressive stresses on the inner and outer sides was particularly pro-

nounced at S3, indicating that local stress distributions cannot be adequately characterized by the average stress across the entire cross-section alone.

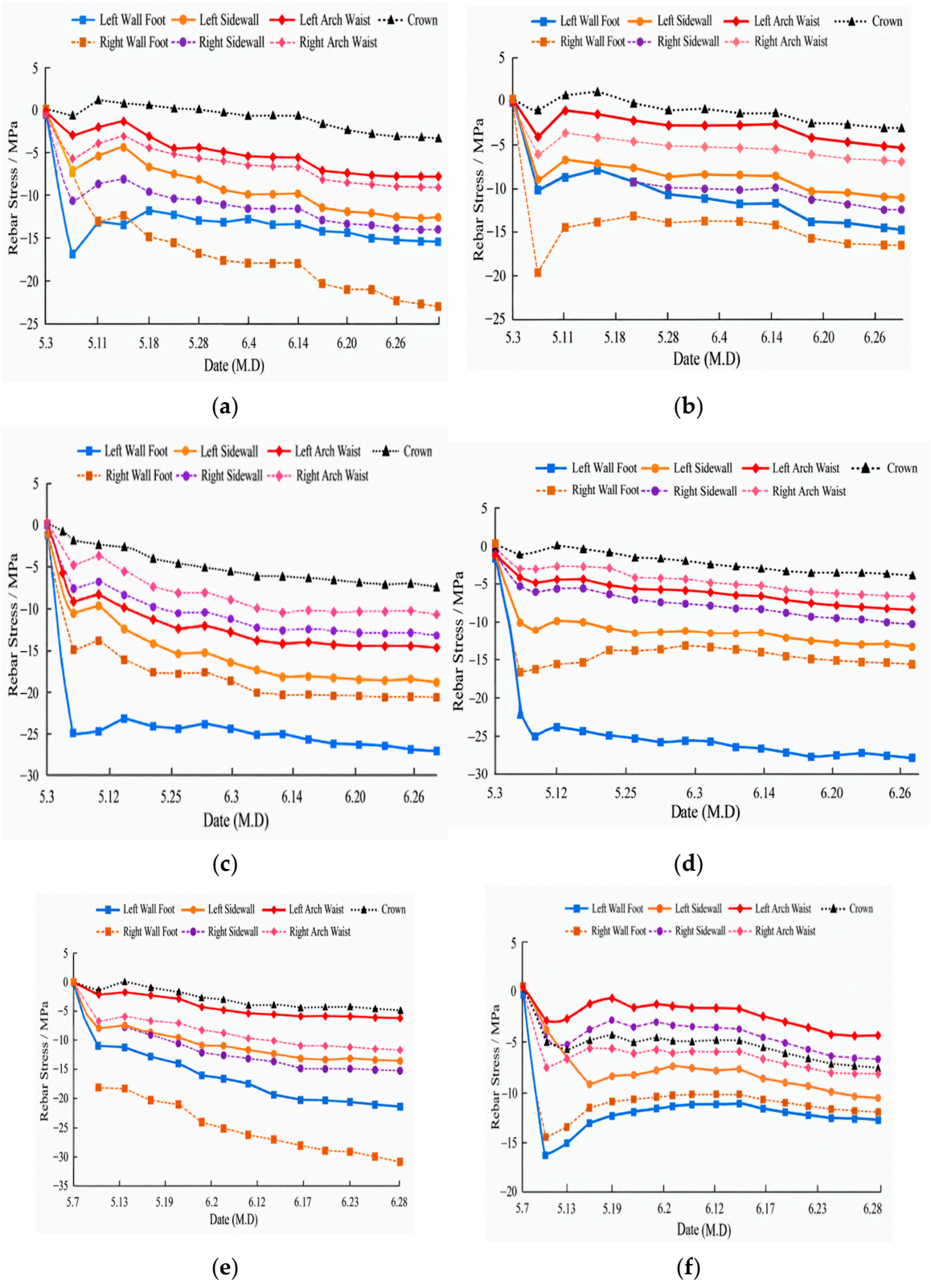


Figure 9. Time histories of reinforcement stress in the inner and outer sides of the secondary lining: (**a**) outer reinforcement at ZK20 + 732; (**b**) inner reinforcement at ZK20 + 732; (**c**) outer reinforcement at ZK20 + 772; (**d**) inner reinforcement at ZK20 + 772; (**e**) outer reinforcement at ZK20 + 783; (**f**) inner reinforcement at ZK20 + 783.

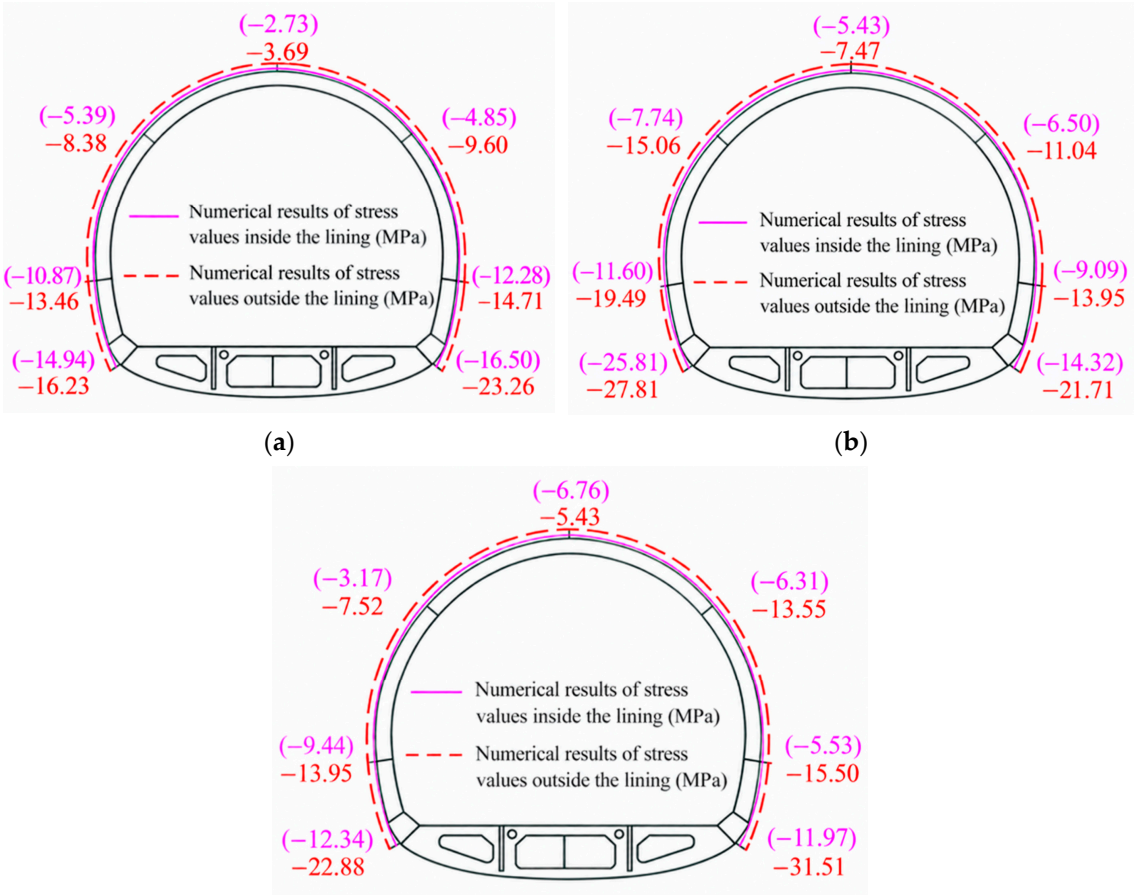


Figure 10. Cross-sectional distribution of reinforcement stress in the secondary lining during the later monitoring stage; positive values indicate tensile stress, and negative values indicate compressive stress (MPa): (**a**) ZK20 + 732; (**b**) ZK20 + 772; (**c**) ZK20 + 783.

Table 4. Summary of reinforcement stress in the secondary lining during the later monitoring stage.

Section	Mean Stress on Inner Side (MPa)	Mean Stress on Outer Side (MPa)	Maximum Compressive Stress on Inner Side (MPa)	Maximum Compressive Stress on Outer Side (MPa)	Ratio of Absolute Mean Stress on Outer Side to Inner Side
S1	−9.65	−12.76	−16.50	−23.26	1.32
S2	−11.50	−16.65	−25.81	−27.81	1.45
S3	−7.93	−15.76	−12.34	−31.51	1.99

Regarding the temporal evolution of reinforcement stress, the normalized rate-of-change analysis indicated that the stress responses at sections S1, S2, and S3 entered slowly varying stages approximately 30, 40, and 25 days, respectively, after casting of the secondary lining of the arch and walls. However, the maximum compressive stresses during the monitoring period occurred approximately 55, 55, and 50 days after casting, respectively. This difference indicates that entering a slowly varying stage does not necessarily imply that the reinforcement stress has reached its final extreme value or that subsequent adjustments have completely ceased. Therefore, both the characteristic transition time and the subsequent stress evolution should be considered when evaluating the mechanical response of the secondary lining.

In summary, the reinforcement in the secondary lining of the arch and walls was predominantly under compression during construction, with nonuniform stress distributions between the inner and outer sides and among different cross-sectional locations. The absolute compressive stresses in the reinforcement at the wall feet and sidewalls were generally higher. However, the interface pressure monitoring results in Section 3.2 showed relatively low normal contact pressure at the wall feet, indicating that these two monitoring indicators did not exhibit a simple correspondence. This suggests that interface contact pressure and internal reinforcement stress reflect different aspects of structural behavior. Local interface pressure alone is insufficient to fully characterize the internal stress state of the lining materials; therefore, concrete stress monitoring results are also needed to further investigate local mechanical differences within the composite lining.

3.4. Concrete Stress in the Secondary Lining of the Arch and Walls

Concrete stress in the secondary lining of the arch and walls exhibited pronounced stage-dependent variations during construction, influenced by monitoring location and differences between the inner and outer sides of the lining. The concrete stress histories for the three representative cross-sections are shown in Figure 11. Overall, the concrete in the secondary lining was predominantly under compression during the monitoring period. Following secondary lining casting, compressive stress increased rapidly at some monitoring points, followed by varying degrees of decline or gradual adjustment. Compared with the inner-side concrete, the outer-side concrete generally exhibited greater stress variations, reflecting nonuniform stress distribution across the lining thickness. Meanwhile, transient or sustained tensile stresses occurred at some monitoring locations, indicating local differences in the stress state of the concrete in the arch and wall lining.

Regarding the nominal stress extremes calculated from the monitored concrete strains, the maximum compressive responses at all three cross-sections occurred during the early stage after secondary lining casting and were mainly concentrated in the outer-side concrete. At section S1, the maximum calculated compressive stress was approximately −6.03 MPa at the outer side of the left haunch, occurring 3 days after casting. At section S2, it was approximately −6.70 MPa at the outer side of the left wall foot, occurring 8 days after casting. At section S3, it was approximately −6.47 MPa at the outer side of the right wall foot, occurring 4 days after casting. Localized tensile responses were also identified. The maximum calculated tensile stresses at sections S1, S2, and S3 were approximately 1.25, 2.34, and 1.43 MPa, respectively, occurring 8, 8, and 11 days after casting. These nominal stress indicators suggest that relatively pronounced concrete strain responses occurred during the early stage after casting, although their magnitudes should be interpreted in light of the limitations of the constant-modulus conversion.

Following secondary lining construction, the concrete stress responses at different monitoring locations exhibited a gradual reduction in their rates of change, although differences among the cross-sections remained. According to the normalized rate-of-change criterion, the concrete stress responses at sections S1, S2, and S3 entered slowly varying stages approximately 40, 40, and 35 days after secondary lining casting, respectively. The corresponding stress extremes and characteristic times are summarized in Table 5. Overall, the concrete stress responses exhibited relatively rapid variations during the initial stage after casting, followed by slower subsequent adjustments. However, the temporal evolution was not fully synchronized among monitoring locations, and the onset of a slowly varying stage should not be interpreted as the complete cessation of local stress changes.

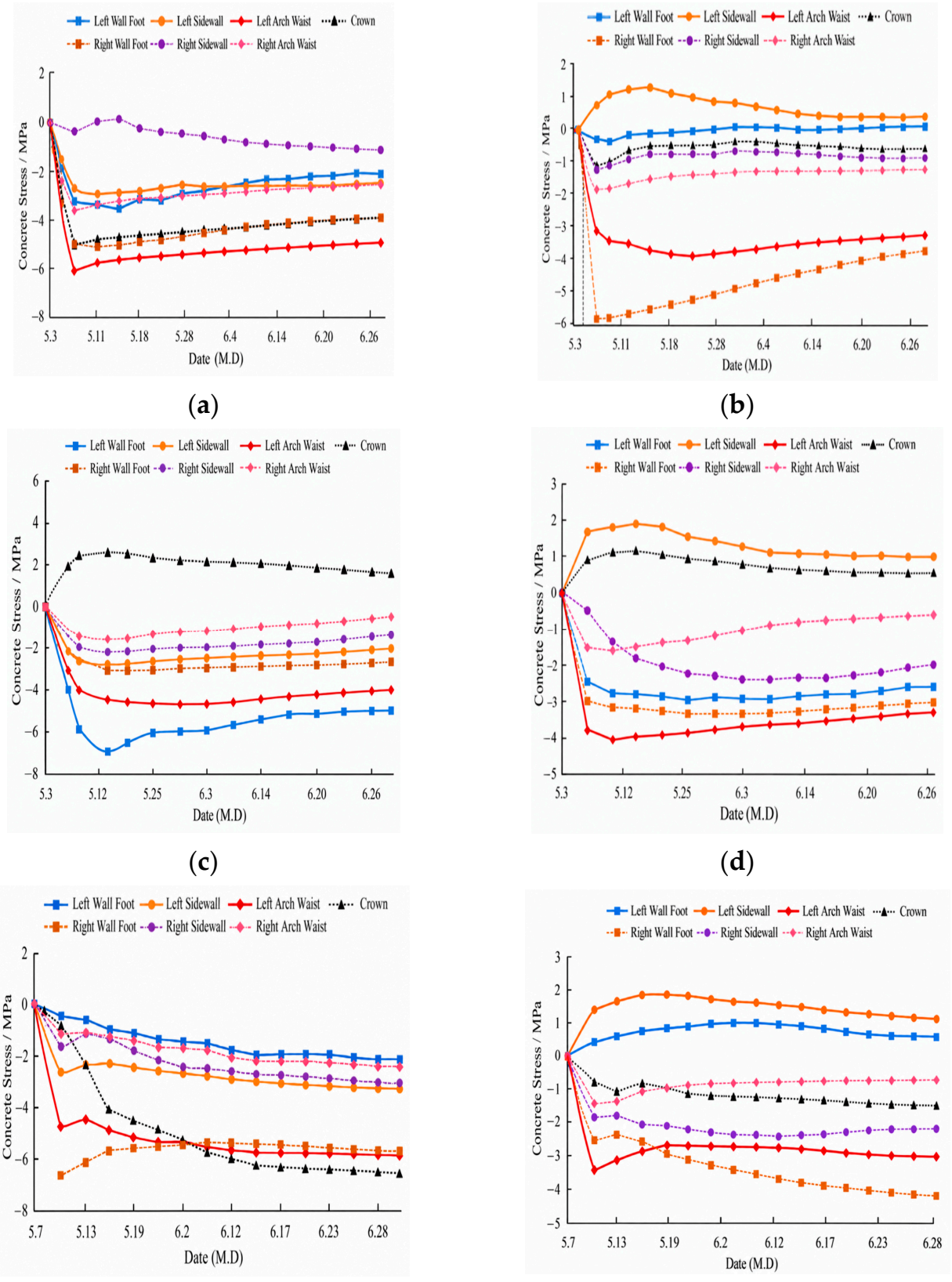


Figure 11. Time histories of concrete stress in the inner and outer sides of the secondary lining: (**a**) outer concrete at ZK20 + 732; (**b**) inner concrete at ZK20 + 732; (**c**) outer concrete at ZK20 + 772; (**d**) inner concrete at ZK20 + 772; (**e**) outer concrete at ZK20 + 783; (**f**) inner concrete at ZK20 + 783.

Table 5. Extreme concrete stresses and temporal characteristics during the monitoring period.

Section	Maximum Compressive Stress (MPa)	Location and Time After Secondary Lining Casting	Maximum Tensile Stress (MPa)	Location and Time After Secondary Lining Casting	Onset of Slowly Varying Stage After Casting (d)
S1	−6.03	Outer left haunch, 3 d	1.25	Inner left sidewall, 8 d	40
S2	−6.70	Outer left wall foot, 8 d	2.34	Outer crown, 8 d	40
S3	−6.47	Outer right wall foot, 4 d	1.43	Inner left sidewall, 11 d	35

To further investigate the spatial distribution of concrete responses, the nominal stresses calculated at the inner and outer monitoring locations during the later monitoring stage were compared, as shown in Figure 12. The calculated responses at all three cross-sections were predominantly compressive, although localized tensile responses were identified. At section S1, the calculated tensile stresses at the inner left wall foot and left sidewall were approximately 0.47 and 0.19 MPa, respectively, while all outer-side monitoring points exhibited compressive responses. At section S2, the corresponding tensile stresses at the inner left sidewall and crown were approximately 0.77 and 0.23 MPa, respectively, whereas the outer crown exhibited a nominal tensile stress of approximately 1.46 MPa. At section S3, the calculated tensile stresses at the inner left wall foot and left sidewall were approximately 0.30 and 0.96 MPa, respectively, while the outer-side monitoring points remained under nominal compression. These results indicate that localized tensile responses may coexist with predominantly compressive behavior, particularly near the wall feet, sidewalls, and crown. However, the calculated tensile values alone are insufficient to confirm the occurrence of concrete cracking.

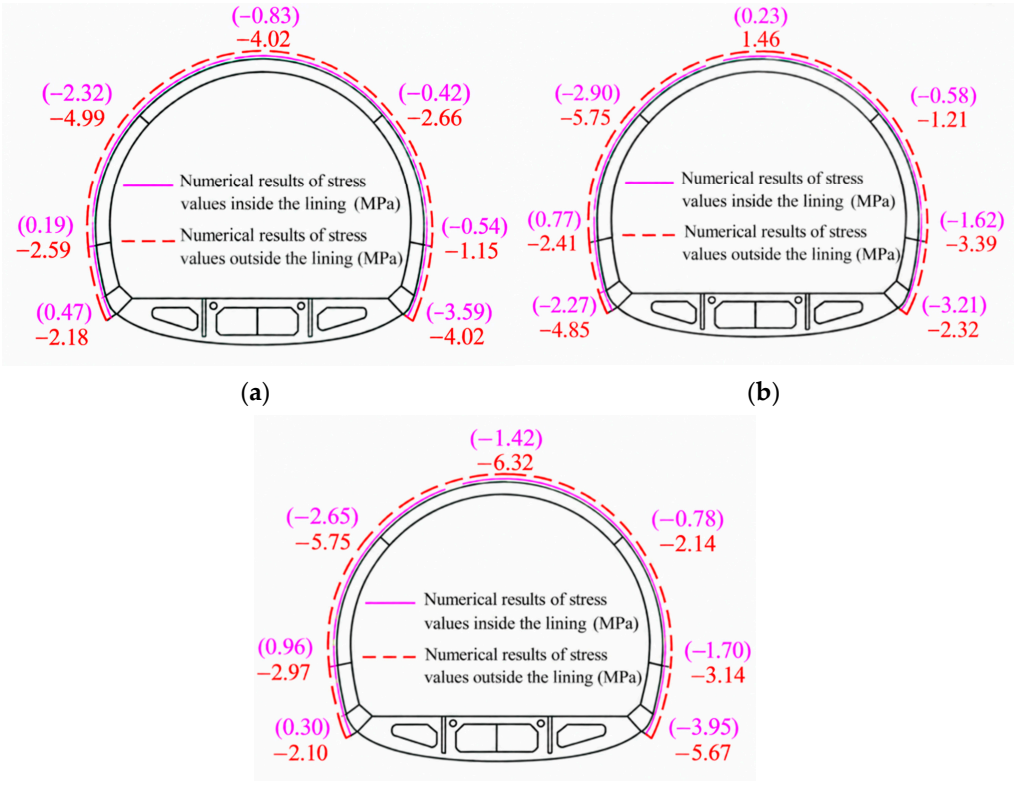


Figure 12. Cross-sectional distribution of concrete stress in the secondary lining during the later monitoring stage (MPa): (**a**) ZK20 + 732; (**b**) ZK20 + 772; (**c**) ZK20 + 783. Positive values indicate tensile stress, and negative values indicate compressive stress.

To further investigate the spatial distribution of the calculated concrete stresses, the average values at compressive monitoring points and the local extremes during the later monitoring stage were analyzed, as summarized in Table 6. The average nominal compressive stresses at the inner-side monitoring points of sections S1, S2, and S3 were approximately −1.54, −2.11, and −2.10 MPa, respectively, while those at the outer-side points were approximately −3.09, −3.32, and −4.02 MPa, respectively. At all three cross-sections, the absolute average compressive stress was greater on the outer side than on the inner side. The differences in these average stress levels remained consistent with those identified using the original elastic modulus because all calculated stress values were rescaled by the same factor. However, as tensile responses occurred at certain monitoring locations, the numbers of points included in the inner- and outer-side compressive averages were not identical. Therefore, these averages characterize the nominal stress responses at selected compressive monitoring points and should not be directly interpreted as the load-sharing proportions of the entire cross-section.

Table 6. Summary of concrete stress in the secondary lining during the later monitoring stage.

Section	Side	Mean Stress at Compressive Monitoring Points (MPa)	Maximum Compressive Stress and Location (MPa)	Tensile Locations and Stresses (MPa)
S1	Inner	−1.54	−3.59, right wall foot	Left wall foot: 0.47; left sidewall: 0.19
S1	Outer	−3.09	−4.99, left haunch	No tensile monitoring points recorded
S2	Inner	−2.11	−3.21, right wall foot	Left sidewall: 0.77; crown: 0.23
S2	Outer	−3.32	−5.75, left haunch	Crown: 1.46
S3	Inner	−2.10	−3.95, right wall foot	Left wall foot: 0.30; left sidewall: 0.96
S3	Outer	−4.02	−6.32, crown	No tensile monitoring points recorded

Regarding the spatial distribution of local compressive responses during the later monitoring stage, the maximum calculated compressive stresses on the inner and outer sides of section S1 were approximately −3.59 MPa at the right wall foot and −4.99 MPa at the left haunch, respectively. At section S2, the corresponding values were approximately −3.21 MPa at the right wall foot and −5.75 MPa at the left haunch. At section S3, they were approximately −3.95 MPa at the right wall foot and −6.32 MPa at the crown. The locations of these extreme responses remained unchanged following the elastic modulus adjustment. The results indicate that the calculated concrete stress responses varied considerably both across the lining thickness and among different transverse locations.

Overall, the strain-derived nominal stress responses of the concrete in the secondary lining of the arch and walls were predominantly compressive during construction, although localized tensile responses were identified at certain monitoring locations. The calculated responses exhibited spatial differences between the inner and outer sides and among different structural locations. Combined with the reinforcement monitoring results in Section 3.3, these findings indicate that both reinforcement and concrete generally exhibited greater compressive responses on the outer side, although their local extreme values did not always occur at the same locations. It should be emphasized that positive nominal tensile stresses calculated from monitored concrete strains do not necessarily indicate the occurrence of concrete cracking. In the present study, the maximum nominal tensile responses occurred approximately 8–11 days after secondary lining casting, when the tensile strength and stiffness of concrete were still developing. Because age-dependent tensile strength measurements and corresponding direct crack observations were not included in the present analysis, the relationship between the calculated tensile stress and the actual

tensile capacity of concrete could not be quantitatively established. Furthermore, the strain-derived stress values may be affected by temperature, shrinkage, creep, and evolving structural restraints. Therefore, the identified tensile regions should be interpreted as locations requiring particular attention during construction rather than confirmed cracking locations. Further evaluation of cracking behavior would require age-specific material testing and direct field crack inspections.

3.5. Crown Settlement and Horizontal Convergence

Cross-sectional deformation is an important indicator of construction disturbance and the restraining effect of the support structure. The crown settlement histories of the three representative cross-sections are shown in Figure 13. Overall, crown settlement accumulated progressively as construction advanced. The deformation trends were broadly similar among the three cross-sections, although the final settlement values differed. The final crown settlements at sections S1, S2, and S3 were 27.50, 33.76, and 29.15 mm, respectively. Section S2 exhibited the greatest settlement, while S1 exhibited the least. Crown settlement mainly occurred during bench excavation and the formation of primary support. As construction progressed, the rate of deformation gradually decreased, although local adjustments occurred in response to subsequent construction activities, demonstrating pronounced stage-dependent evolution.

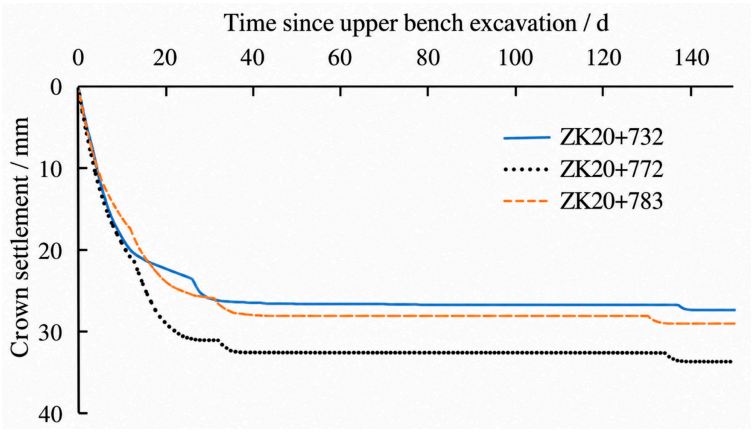


Figure 13. Time histories of crown settlement at the three cross-sections.

To further investigate the influence of construction stages on crown deformation, the settlement rates at the three cross-sections were compared, as shown in Figure 14 and Table 7. The maximum settlement rates at sections S1, S2, and S3 were 2.75, 3.12, and 3.08 mm/d, respectively, all occurring during the rapid deformation stage in the early construction period. Based on construction events and changes in the settlement-rate curves, crown settlement can be divided into several stages: rapid deformation following upper-bench excavation, renewed acceleration caused by middle-bench excavation, a declining settlement rate after lower-bench construction, and further adjustments following invert excavation and assembly. Changes in deformation rates showed temporal associations with the construction sequence. In particular, settlement rates increased noticeably after bench excavation and then gradually declined, reflecting the staged response of cross-sectional deformation to excavation disturbances and changes in support constraints.

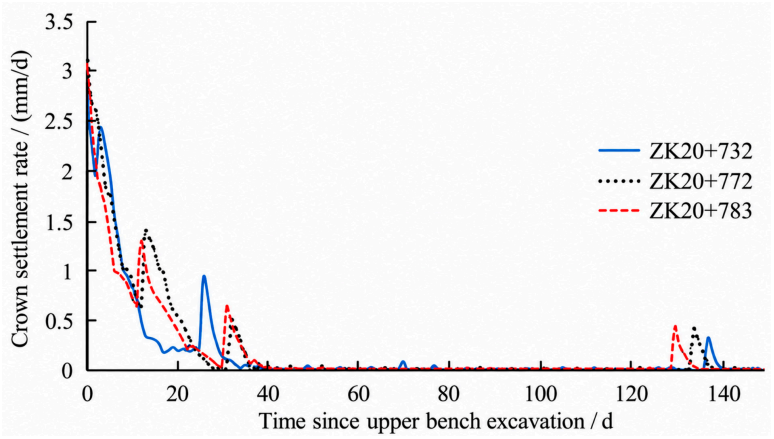


Figure 14. Time histories of crown settlement rates at the three cross-sections.

Table 7. Magnitudes and temporal characteristics of crown settlement.

Section	Final Settlement (mm)	Maximum Settlement Rate (mm/d)	Onset of Initial Slowly Varying Stage After Upper-Bench Excavation (d)	Onset of Slowly Varying Stage After Invert Excavation (d)
S1	27.50	2.75	35	4
S2	33.76	3.12	36	5
S3	29.15	3.08	38	5

As shown in Table 7, the crown settlement responses at sections S1, S2, and S3 entered an initial slowly varying stage approximately 35, 36, and 38 days after upper-bench excavation, respectively, as identified using the normalized rate-of-change criterion. As subsequent bench excavation and invert construction proceeded, crown settlement continued to adjust. Following invert excavation and rapid assembly of the precast components, the crown settlement responses at sections S1, S2, and S3 entered slowly varying stages after approximately 4, 5, and 5 days, respectively, as identified using the normalized rate-of-change criterion. This indicates a temporal association between changes in structural restraint during invert construction and the gradual stabilization of cross-sectional deformation. As the bottom precast components were installed and the support system progressively formed, the rate of deformation decreased. However, this temporal relationship alone is insufficient to quantify the reduction in deformation attributable to the precast invert relative to other construction methods.

In addition to crown settlement, horizontal convergence provides information on tunnel cross-sectional deformation during different excavation stages. The horizontal convergence histories at the upper, middle, and lower benches of the three representative cross-sections are shown in Figure 15. Overall, horizontal convergence at all three benches accumulated progressively during construction, with pronounced differences in deformation magnitude and development among measurement lines at different heights. The final upper-bench horizontal convergence values at sections S1, S2, and S3 were 30.68, 22.29, and 22.93 mm, respectively, while the corresponding lower-bench values were 14.72, 12.52, and 12.24 mm. At each cross-section, horizontal convergence was greatest at the upper bench and smallest at the lower bench, with the middle bench exhibiting intermediate values. This demonstrates a nonuniform deformation pattern along the height of the tunnel cross-section.

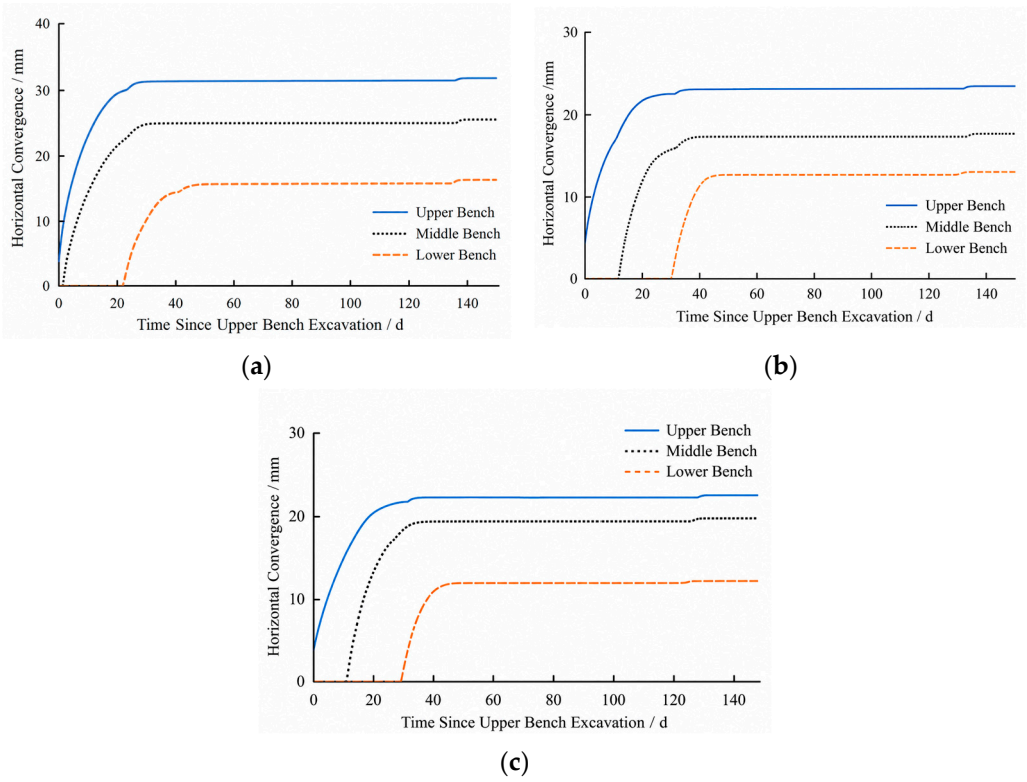


Figure 15. Time histories of horizontal convergence at the upper, middle, and lower benches of each cross-section: (**a**) ZK20 + 732; (**b**) ZK20 + 772; (**c**) ZK20 + 783.

As shown in Figure 16 and Table 8, the horizontal convergence rate varied in stages as excavation progressed at each bench, increasing rapidly after excavation and then gradually decreasing. The maximum convergence rates at sections S1, S2, and S3 were 3.08, 2.16, and 2.53 mm/d, respectively. Based on the normalized rate-of-change criterion, the horizontal convergence responses at sections S1, S2, and S3 entered an initial slowly varying stage approximately 52, 47, and 45 days, respectively, after upper-bench excavation. Because the excavation and support installation sequences differed among the benches, the cumulative convergence at the upper bench was generally greater than that at the lower bench. Following invert excavation and rapid assembly of the precast components, horizontal convergence at sections S1, S2, and S3 entered slowly varying stages after approximately 5, 5, and 4 days, respectively, based on the same normalized rate-of-change criterion. This behavior was broadly consistent with the staged evolution of crown settlement.

Table 8. Magnitudes and temporal characteristics of horizontal convergence at different benches.

Section	Final Upper-Bench Convergence (mm)	Final Lower-Bench Convergence (mm)	Maximum Convergence Rate (mm/d)	Onset of Initial Slowly Varying Stage After Upper-Bench Excavation (d)	Onset of Slowly Varying Stage After Invert Excavation (d)
S1	30.68	14.72	3.08	52	5
S2	22.29	12.52	2.16	47	5
S3	22.93	12.24	2.53	45	4

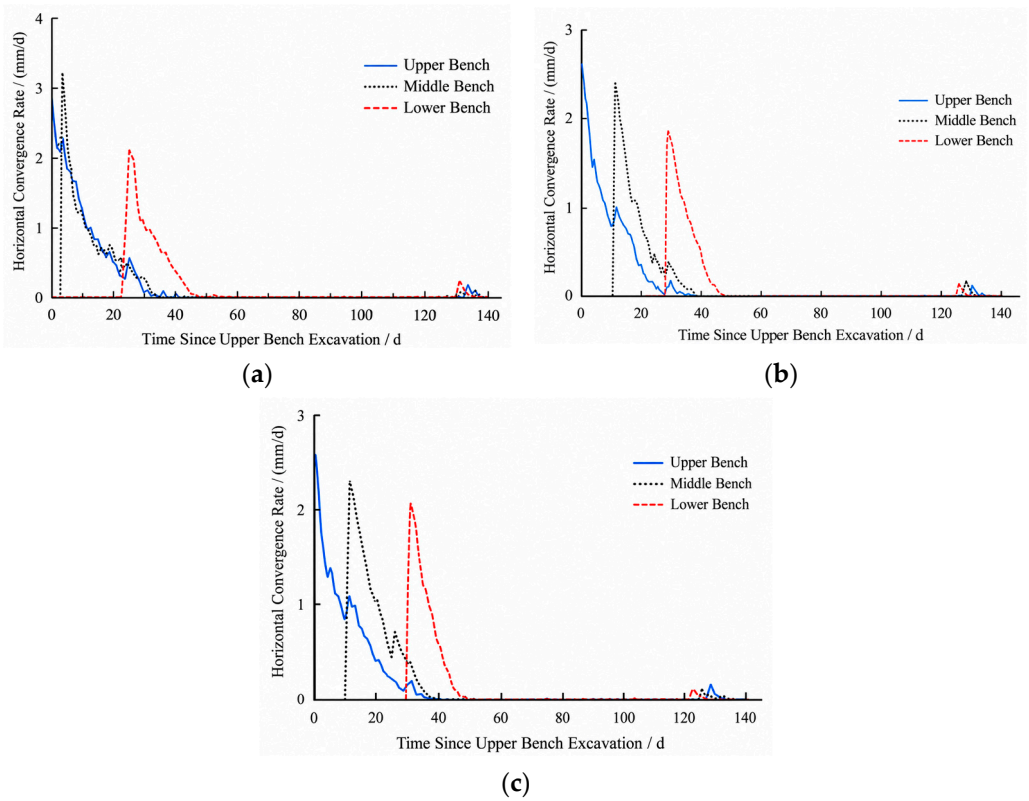


Figure 16. Time histories of horizontal convergence rates at the upper, middle, and lower benches: (**a**) ZK20 + 732; (**b**) ZK20 + 772; (**c**) ZK20 + 783.

The final crown settlement and horizontal convergence at all three sections remained below the deformation control limit of 75 mm adopted for this project. The maximum crown settlement was 33.76 mm, corresponding to 45.0% of the control limit, while the maximum horizontal convergence was 30.68 mm, corresponding to 40.9%. The maximum crown settlement occurred at section S2, whereas the maximum horizontal convergence occurred at section S1, indicating that the spatial distributions of vertical and horizontal deformation were not completely consistent. Overall, cross-sectional deformation accumulated in stages as excavation progressed and entered a slowly varying stage approximately 4–5 days after rapid invert assembly. However, the stabilization of overall deformation does not necessarily indicate that subsequent adjustments in local structural forces have ceased.

4. Discussion

4.1. Construction Events and Interfacial Load Transfer

The interfacial contact pressure in the composite lining incorporating a precast invert exhibited stage-dependent variations that were temporally associated with construction activities. Increases and decreases in contact pressure at several monitoring locations coincided with the entry and departure of construction equipment, respectively. These observations suggest that temporary construction loads may influence the contact conditions between the precast invert and the underlying cushion layer. However, temporal correspondence alone is insufficient to establish a direct causal relationship. Other factors, including spatially nonuniform interface contact, changes in surrounding rock and support conditions, and concurrent construction disturbances, may also contribute to the observed pressure variations. Previous studies have indicated that construction loads and evolving structural constraints can affect the mechanical response of tunnel linings [15]. Nevertheless, the present monitoring data do not allow the individual contributions of these factors

to be isolated or quantified. Accordingly, the relationships between construction events and contact pressure variations are interpreted as temporal associations supported by plausible mechanical explanations, rather than conclusively demonstrated causal mechanisms.

Differences in invert–cushion contact pressure were observed between the available monitoring records before and after the interruption covering the base grouting period. However, because no continuous measurements were available during this interval, the contribution of grouting to the observed pressure changes could not be isolated from other possible influences, including variations in interface support conditions and construction disturbances. Accordingly, the observed differences are interpreted as changes in the interface contact state between two monitoring periods, rather than as direct evidence of a grouting-induced pressure increment. Subsequent pressure adjustments recorded after the casting of the secondary lining are analyzed separately based on the available monitoring histories. In addition, the relatively low contact pressure recorded at some wall-foot locations may be related to local contact conditions and connection details [7,9]. Nevertheless, this observation alone is insufficient to establish the presence of interface gaps or connection damage. Overall, construction-stage changes are closely associated with interfacial load transfer, and local contact conditions should be evaluated by considering multiple monitoring indicators.

The differences in contact pressure among the three monitoring cross-sections may be associated with the combined effects of ground–support interaction, local interface contact conditions, and construction-stage boundary conditions. The tunnel mainly passes through mudstone interbedded with sandstone and is situated in sloping terrain, where variations in surrounding rock conditions and overburden may influence the distribution of loads acting on the lining. In addition, differences in primary support restraint, local contact stiffness, and construction disturbances may contribute to the nonuniform pressure responses. Although S1 exhibited a substantially higher local pressure peak than S2 and S3, the peak pressures occurred at different circumferential locations, indicating that the interface response was spatially heterogeneous. The available monitoring records do not provide sufficient section-specific information on overburden, groundwater conditions, and surrounding rock properties to independently quantify the contributions of these factors. Therefore, the elevated pressure at the left haunch of S1 is interpreted as a localized interface response potentially influenced by multiple interacting conditions rather than the result of a single identified cause.

4.2. Spatial Differences Between Contact Pressure and Material Stress

Interface contact pressure and internal lining material stresses exhibited different spatial distributions. During the later monitoring stage, the normal contact pressures at the right wall foot were 42.35, 21.32, and 25.26 kPa at sections S1, S2, and S3, respectively. At section S3, the outer reinforcement at the right wall foot exhibited a compressive stress of −31.51 MPa, while the strain-derived nominal concrete stresses at the inner and outer sides of the same location were approximately −3.95 and −5.67 MPa, respectively. The contact pressure reflects the local normal interaction between the secondary lining and primary support, whereas reinforcement and concrete stresses characterize the internal mechanical response of the lining. Internal stress distributions may be influenced by the combined effects of axial forces, bending moments, structural geometry, and connection restraints, and therefore do not necessarily correspond directly to the local interface-normal pressure. Previous studies have also demonstrated the influence of connection stiffness on internal load-transfer characteristics [10]. These observations indicate that the mechanical state of the wall-foot region should be evaluated by considering both interface contact conditions and internal material stresses.

The monitoring results for reinforcement and concrete exhibited distinct spatial variations, with relatively greater compressive stress magnitudes generally observed on the outer side of the secondary lining. Based on the adopted linear–elastic conversion, localized positive strain-derived nominal stress responses were identified at several concrete monitoring locations, indicating potentially critical tensile regions. However, the interpretation of these calculated responses requires consideration of early-age concrete behavior. In particular, the development of the elastic modulus, hydration-related temperature variations, autogenous and drying shrinkage, creep, and evolving structural restraints may all influence the measured strain and its conversion into stress [21–23].

In this study, a constant reference elastic modulus of 32.5 GPa was adopted for the C40 concrete in the secondary lining. As the time-dependent material properties and non-mechanical strain components were not independently quantified, the calculated stresses should be interpreted as approximate strain-derived indicators rather than direct measurements of actual mechanical stresses. Notably, the maximum calculated nominal tensile stress of approximately 2.34 MPa at section S2 occurred eight days after secondary lining casting, when the tensile strength and stiffness of the concrete were still developing. Without corresponding age-dependent tensile strength measurements and direct crack observations, the calculated tensile responses cannot be used to confirm the occurrence of cracking or quantitatively evaluate the cracking safety margin. Therefore, the results are primarily used to characterize relative spatial differences, temporal evolution, and potentially critical regions requiring further monitoring.

4.3. Timescales of Deformation Stabilization and Stress Adjustment

The monitoring results indicate that overall deformation and local mechanical responses exhibit distinct temporal evolution characteristics during construction. Based on the normalized rate-of-change criterion, crown settlement and horizontal convergence entered slowly varying stages approximately 4–5 days after invert excavation and rapid assembly, whereas interface contact pressure and lining material stress entered slowly varying stages approximately 24–40 days after the subsequent casting of the secondary lining. It should be emphasized that these characteristic times are referenced to different construction events and therefore cannot be directly compared as equivalent stabilization periods. Furthermore, the identified times represent transitions to relatively slow response stages rather than complete mechanical stabilization. Nevertheless, these observations demonstrate that a substantial reduction in the overall deformation rate does not necessarily indicate the cessation of subsequent local stress adjustments.

The reduction in the observed deformation rate following invert construction was temporally associated with the installation of the bottom structure and changes in structural constraints. Similar construction-stage interactions in structures incorporating precast inverts have been discussed in previous research [25]. However, the present study did not include a contemporaneous conventional cast-in-place invert section with comparable geological conditions, structural configurations, and construction sequences. Therefore, the observed deformation characteristics cannot be attributed exclusively to the precast invert construction method, and the relative contributions of the construction method and other influencing factors cannot be independently quantified. More importantly, the available field monitoring data do not provide sufficient evidence to establish the superiority of the precast invert system over a conventional cast-in-place invert in terms of deformation control, structural performance, or construction efficiency. Accordingly, the results should be interpreted as a characterization of the mechanical responses of the investigated composite lining during construction, rather than as a direct comparison between alternative invert construction methods. Taken together, these observations suggest that overall de-

formation measurements alone are insufficient to characterize the complete mechanical response of composite linings during construction. A complementary monitoring strategy is therefore recommended, in which crown settlement and horizontal convergence are used to evaluate overall deformation, while interface contact pressure and reinforcement and concrete stress measurements are used to identify localized mechanical responses. Particular attention should be paid to the wall feet, sidewalls, and regions exhibiting tensile stress, and local stress monitoring should continue even after the overall deformation response has entered a slowly varying stage. This approach may provide a more comprehensive basis for construction-stage structural assessment than reliance on an individual monitoring indicator.

It should be acknowledged that the present study is based on field monitoring data from three cross-sections of a single tunnel, which imposes certain limitations on the generalizability of the findings. Although comparisons among the three cross-sections provide insights into the spatial differences and stage-dependent evolution of the monitored responses, they do not constitute independent validation under different engineering conditions. Furthermore, no additional tunnel case, numerical simulation, or dedicated experimental investigation was available to independently verify the inferred mechanical mechanisms. Therefore, the findings should be interpreted primarily as project-specific observations rather than universally applicable conclusions. Variations in geological conditions, structural configurations, and construction sequences may influence the mechanical responses of composite linings with prefabricated inverts. Future research should incorporate monitoring data from multiple engineering projects and combine field observations with numerical analyses or experimental investigations to further validate the identified response characteristics and evaluate their applicability under different engineering conditions.

5. Conclusions

Taking the precast invert construction section of Yaopocun Tunnel on the Tianlong Railway as the engineering case, this study analyzed archived field monitoring data from three representative cross-sections. The mechanical responses and stage-dependent evolution of the composite lining consisting of a precast invert and cast-in-place arch and wall lining were investigated in terms of interfacial contact pressure, lining material stress, and cross-sectional deformation. The following conclusions were drawn:

(1) Interfacial contact pressure in the composite lining incorporating a precast invert underwent stage-dependent adjustments and exhibited pronounced spatial nonuniformity. The presence and removal of construction equipment were associated with increases and decreases, respectively, in contact pressure beneath the invert. Further adjustments occurred after casting of the secondary lining of the arch and walls. During the later monitoring stage, the mean monitored pressures at the invert–cushion interface ranged from 30.39 to 36.47 kPa, while those at the secondary lining–primary support interface ranged from 52.67 to 85.16 kPa. The locations of the maximum local pressures differed among the cross-sections. Because base grouting occurred during a monitoring gap, the instantaneous pressure change attributable to grouting could not be independently quantified using the available data.

(2) Internal lining material stresses exhibited spatial distributions that differed from those of interface contact pressure. During the later monitoring stage, all reinforcement monitoring points were under compression. The absolute average compressive stress on the outer side was 1.32–1.99 times that on the inner side, with relatively high compressive stresses generally occurring at the wall feet and sidewalls. At all three cross-sections, contact pressure at the wall feet was relatively low, while local reinforcement compressive stresses were relatively high. This indicates that interface contact pressure

and internal lining material stress do not exhibit a simple correspondence. Interface pressure alone is therefore insufficient to fully characterize the local mechanical state of the composite lining.

(3) The strain-derived nominal stress responses of the concrete in the secondary lining were predominantly compressive, with localized tensile responses observed at certain monitoring locations. The maximum calculated tensile stresses at the three cross-sections ranged from approximately 1.25 to 2.34 MPa, while the maximum value during the later monitoring stage was approximately 1.46 MPa. These results indicate that localized tensile responses may persist during the subsequent adjustment of the lining structure. Particular attention should therefore be paid to the wall feet, sidewalls, and crown regions exhibiting tensile responses during construction. The calculated tensile stresses provide a basis for identifying potentially critical regions but are insufficient on their own to confirm concrete cracking.

(4) Overall deformation and local mechanical responses in the composite lining incorporating a precast invert exhibited different stage-dependent evolution patterns. The final crown settlement at the three cross-sections ranged from 27.50 to 33.76 mm, and the final upper-bench horizontal convergence ranged from 22.29 to 30.68 mm. Both remained below the project deformation control limit of 75 mm. Based on the proposed normalized rate-of-change criterion, cross-sectional deformation entered slowly varying stages approximately 4–5 days after invert excavation and rapid assembly, while interface contact pressure and lining material stress entered slowly varying stages approximately 24–40 days after secondary lining casting. As these characteristic times were referenced to different construction events, they should not be interpreted as directly comparable stabilization periods. The findings indicate that the onset of a slowly varying deformation stage does not necessarily imply the cessation of subsequent local mechanical adjustments. Accordingly, construction-stage monitoring should not be terminated solely because overall deformation has entered a slowly varying stage. Continued monitoring of stress evolution at the wall feet, sidewalls, and localized tensile regions is also necessary.

It should be noted that these conclusions are derived from field monitoring data obtained from a single tunnel project. Although the findings provide engineering insights into the construction-stage behavior of composite linings with prefabricated inverts, their applicability to different geological conditions, structural configurations, and construction methods requires further verification through independent field investigations, numerical analyses, or experimental studies.

These conclusions are based on field monitoring data from three representative cross-sections within a single tunnel project. Because no contemporaneous cast-in-place invert control section was available, the observed deformation responses cannot be used to establish the comparative superiority of the precast invert system in terms of deformation control or structural performance. The findings therefore provide project-specific evidence of the construction-stage mechanical behavior of the investigated composite lining rather than a quantitative comparison of alternative invert construction methods. Further studies involving independent engineering cases, comparable cast-in-place invert sections, and complementary numerical or experimental investigations are needed to validate the identified response characteristics and assess their broader applicability.

Author Contributions: Conceptualization, C.C. and C.S.; methodology, Y.L., C.C. and C.S.; software, Y.L. and B.W.; validation, C.C., C.X. and Y.L.; formal analysis, Y.L. and B.W.; investigation, C.C., C.X. and Y.L.; resources, C.C. and C.X.; data curation, Y.L. and B.W.; writing—original draft preparation, C.C. and Y.L.; writing—review and editing, C.C., Y.L., C.X., B.W. and C.S.; visualization, Y.L. and B.W.; supervision, C.S.; project administration, C.C. and C.S. All authors have read and agreed to the published version of the manuscript.

Funding: This research was financially supported by Shandong Expressway Infrastructure Construction Co., Ltd.

Data Availability Statement: The data supporting the findings of this study are available from the corresponding author upon reasonable request.

Acknowledgments: The authors acknowledge Shandong Expressway Infrastructure Construction Co., Ltd. for providing relevant engineering information, on-site information, and assistance from its technical personnel during this study.

Conflicts of Interest: The authors declare that this study received financial support from Shandong Expressway Infrastructure Construction Co., Ltd. The funder was involved in the research by providing financial support, relevant engineering and on-site information, and technical assistance. Authors C.C. and C.X. are affiliated with the funding company and contributed to the study as described in the Author Contributions section. These financial and institutional relationships are disclosed to ensure transparency regarding the role of the funder in the research.

References

1. Brown, E.T.; Bray, J.W.; Ladanyi, B.; Hoek, E. Ground response curves for rock tunnels. *J. Geotech. Eng.* **1983**, *109*, 15–39. [CrossRef]
2. Carranza-Torres, C.; Fairhurst, C. Application of the convergence-confinement method of tunnel design to rock masses that satisfy the Hoek-Brown failure criterion. *Tunn. Undergr. Space Technol.* **2000**, *15*, 187–213. [CrossRef]
3. Wang, F. Mechanical characteristics of prefabricated inverted arch during hoisting in mining-method tunnels. *J. Railw. Eng. Soc.* **2022**, *39*, 79–85.
4. Liu, J.; Wang, Y.; Qiu, C.; Qu, L.; Yuan, W.; Du, Y.; Hao, Y. Optimal design of prefabricated inverted arch structure for highway tunnels. *J. Hohai Univ. (Nat. Sci.)* **2023**, *51*, 55–64. [CrossRef]
5. Wang, Y.; Xu, H.; Hao, Y.; Zhou, X.; Liu, J.; Li, Y. Model test research on deformation and failure of box-shaped prefabricated inverted arch structure of highway tunnels. *J. Zhejiang Univ.-Sci. A* **2024**, *58*, 1417–1426. [CrossRef]
6. Kong, C.; Gao, X.; Wang, F.; Wang, H.; Li, H.; Zhao, X.; Liu, J.; Zhang, Y.; Luo, Y. Analysis of mechanical properties and joint selection for secondary linings in drill-and-blast tunnels with prefabricated invert arch: Case study of a single-line railway tunnel. *Tunn. Undergr. Space Technol.* **2024**, *144*, 105560. [CrossRef]
7. Deng, Q.; Fu, J.; Gao, W. Study on structural selection and force characteristics of assembled inverts in drill-and-blast tunnels. *Trans. Beijing Inst. Technol.* **2026**, *46*, 131–140. [CrossRef]
8. Chen, Z.; Liang, Y.; Ye, P.; Zhang, S. Experimental and finite element analysis on the mechanical performance of prefabricated invert-to-lining joints in large-section highway tunnels under direct shear loading. *Structures* **2024**, *59*, 105764. [CrossRef]
9. Zhang, S.; Ma, M.; Li, C.; Ye, P.; Chen, Z. Experimental study on shear performance of longitudinal joints in prefabricated invert arches for mountain mining-method tunnels. *Materials* **2025**, *18*, 3025. [CrossRef] [PubMed]
10. Guan, Z.; Deng, T.; Wang, G.; Jiang, Y. Studies on the key parameters in segmental lining design. *J. Rock Mech. Geotech. Eng.* **2015**, *7*, 674–683. [CrossRef]
11. Teachavorasinskun, S.; Chub-uppakarn, T. Influence of segmental joints on tunnel lining. *Tunn. Undergr. Space Technol.* **2010**, *25*, 490–494. [CrossRef]
12. Jin, Y.; Ding, W.; Yan, Z.; Soga, K.; Li, Z. Experimental investigation of the nonlinear behavior of segmental joints in a water-conveyance tunnel. *Tunn. Undergr. Space Technol.* **2017**, *68*, 153–166. [CrossRef]
13. Cavalaro, S.H.P.; Blom, C.B.M.; Walraven, J.C.; Aguado, A. Structural analysis of contact deficiencies in segmented lining. *Tunn. Undergr. Space Technol.* **2011**, *26*, 734–749. [CrossRef]
14. Liu, X.; Dong, Z.; Bai, Y.; Zhu, Y. Investigation of the structural effect induced by stagger joints in segmental tunnel linings: First results from full-scale ring tests. *Tunn. Undergr. Space Technol.* **2017**, *66*, 1–18. [CrossRef]
15. Chen, J.-S.; Mo, H.-H. Mechanical behavior of segment rebar of shield tunnels during construction. *J. Zhejiang Univ.-Sci. A* **2008**, *9*, 888–899. [CrossRef]
16. Pham, A.T.; Sugimoto, M. The effects of tangential ground–lining interaction on segmental lining behavior using the beam-spring model. *Appl. Sci.* **2020**, *10*, 1084. [CrossRef]

17. Zhang, D.; Fang, Q.; Li, P.; Wong, L.N.Y. Structural responses of secondary lining of high-speed railway tunnels excavated in loess ground. *Adv. Struct. Eng.* **2013**, *16*, 1371–1379. [CrossRef]
18. Wu, Y.; Zhuang, G.; Liang, W.; Huang, L. Safety analysis of secondary lining of Yulinzi Tunnel based on field monitoring. *Appl. Sci.* **2023**, *13*, 8328. [CrossRef]
19. Zhang, H.; Hao, Z.; Ge, Z.; Zhang, G.; Chen, S.; Wang, L. Construction mechanical behavior and deformation characteristics of lining structures: A case study of large-span and small-clearance tunnels. *Structures* **2022**, *45*, 2007–2021. [CrossRef]
20. Hu, X.; Nan, X.; Zhang, W.; Zhu, D. Evolution of mechanical behavior of secondary linings during construction of large-span tunnels. *J. Highw. Transp. Res. Dev.* **2024**, *41*, 151–162. [CrossRef]
21. Bouabdallah, A.; Benaissa, A.; Bouabdallah, M.-A.; Malab, S.; Khatir, A. Development and performance evaluation of self-leveling sand concrete: Enhanced fluidity, mechanical strength, durability, and non-destructive analysis. *Constr. Build. Mater.* **2025**, *468*, 140463. [CrossRef]
22. Bouabdallah, A.; Khatir, A.; Bouabdallah, M.-A.; Bouchama, A. Microstructural characterization of an optimized self-leveling sand concrete: Correlating SEM, EDS and XRD observations with mechanical performance. *Constr. Build. Mater.* **2026**, *543*, 148145. [CrossRef]
23. Rankoth, C.K.; Hosoda, A.; Iwama, K. Modeling and verification of early-age thermal stress in second lining concrete of NATM tunnels. *J. Adv. Concr. Technol.* **2017**, *15*, 213–226. [CrossRef]
24. Nakamura, A.; Kunichika, M.; Kameya, H.; Nakamura, H. Identification of thermal properties for initial crack prediction in tunnel lining concrete and its analysis. *J. JSCE Ser. F1 (Tunn. Eng.)* **2015**, *70*, I_1–I_16. [CrossRef] [PubMed]
25. Sun, M.; Guan, Z.; Guo, C.; Xi, X.; Tian, S. Influence of the waterproof layer on lining mechanical performance under early temperature loading. *PLoS ONE* **2025**, *20*, e0321143. [CrossRef] [PubMed]
26. Song, W.; Lai, H.; Liu, Y.; Yang, W.; Zhu, Z. Field and laboratory study of cracking and safety of secondary lining for an existing highway tunnel in loess ground. *Tunn. Undergr. Space Technol.* **2019**, *88*, 35–46. [CrossRef]
27. Khatir, A.; Oulad Brahim, A.; Capozucca, R.; Khatir, S.; Noori, M.; Sarhosis, V.; Bhowmik, B.; Cuong-Le, T. Structural recovery and damage prediction in GFRP-BFRP patched plates using hybrid SSA-SCA-XGBoost model and vibration data. *Compos. Struct.* **2026**, *393*, 120638. [CrossRef]
28. Khatir, A.; Capozucca, R. Artificial, convolutional, and deep neural networks for structural health monitoring: A review. *HCMCOU J. Sci. Adv. Comput. Struct.* **2026**, *16*, 7–50. [CrossRef]
29. Wang, M.; Du, Y.; Lai, J.; Shi, X.; Ma, E.; Sun, H.; Qiu, J. Mechanical properties of a novel prefabricated inverted arch in NATM tunnels: Insights from numerical experiments and in situ tests. *Tunn. Undergr. Space Technol.* **2026**, *173*, 107476. [CrossRef]
30. Hu, S.; Yang, W.; Bian, L.; Wang, H.; Kong, D.; Zhao, J. Damage analysis of bridge piers under rapid flow based on the concrete damaged plasticity model. *Transp. Res.* **2023**, *9*, 143–152. [CrossRef]
31. *GB 50010-2010*; Code for Design of Concrete Structures. China Architecture and Building Press: Beijing, China, 2010.

Disclaimer/Publisher's Note: The statements, opinions and data contained in all publications are solely those of the individual author(s) and contributor(s) and not of MDPI and/or the editor(s). MDPI and/or the editor(s) disclaim responsibility for any injury to people or property resulting from any ideas, methods, instructions or products referred to in the content.